PICOSECOND AND SUBPICOSECOND MEASUREMENTS

CHUNG-YEE LEUNG

INSTITUTE OF ELECTRO-OPTICAL SICNECES
NATIONAL CENTRAL UNIVERSITY
CHUNG-LI, TAIWAN 320, REPUBLIC OF CHINA

in

Proceedings of the 1983 International School and Symposium on Precision Measurement and Gravity Experiment, Taipei, Republic of China, January 24 - February 2, 1983, ed. by W.-T. Ni (Published by National Tsing Hua University, Hsinchu, Taiwan, Republic of China, June, 1983)

OUTLINE

PICOSECOND AND SUBPICOSECOND MEASUREMENTS

Chung-Yee Leung
Institute of Electro-Optical Sciences
National Central University
Chung-Li, Taiwan 320
Republic of China

ABSTRACT

This paper gives a review of picosecond and subpicosecond measurement techniques using ultrashort optical pulses from modelocked laser systems. Availability of these short pulses has provided researchers a powerful tool for the study of ultrafast phenomena, where direct measurements in the time domain were not possible before. Generation methods and measurement schemes are described. Recent rapid progress in the area of opto-electronic measurement techniques using high speed photoconductors is also discussed.

1. Introduction

Record of man's interest in accurate measurements of high speed phenomena dates back to the time of Galilei, when he used his pulse to time brief events. Since that time, the ability to measure short intervals has advanced from 1 second to tens of femtoseconds (10^{-15} sec). Fig.1 shows the progress. Most notable from Fig.1 is the sharp improvement in the past two decades, relating to rapid advances in the capability of lasers to produce ultrashort pulses. Until 1965, the shortest time interval which could be measured was limited to about 1 nanosecond (10^{-9} sec). With the invention of mode-locking lasers, this capability suddenly increased by 3 orders of magnitude to the picosecond (10^{-12} sec) regime. When Fig.1 was drawn in 1977 [1], the shortest pulse generated was about 0.3 psec [2]. Recent progress has allowed us to put another point in that figure below the 10^{-13} sec mark [3,4].

Availability of picosecond and subpicosecond optical pulses has provided scientists a powerful research tool for the probing of ultrafast phenomena where direct measurements in the time domain were previously impossible. Today, research activities in this field is blooming. Studies of a wide variety of ultrafast phenomena in physics, chemistry, biology and engineering, covering all sorts of materials : solids liquids, gases and plasmas have been carried. out.

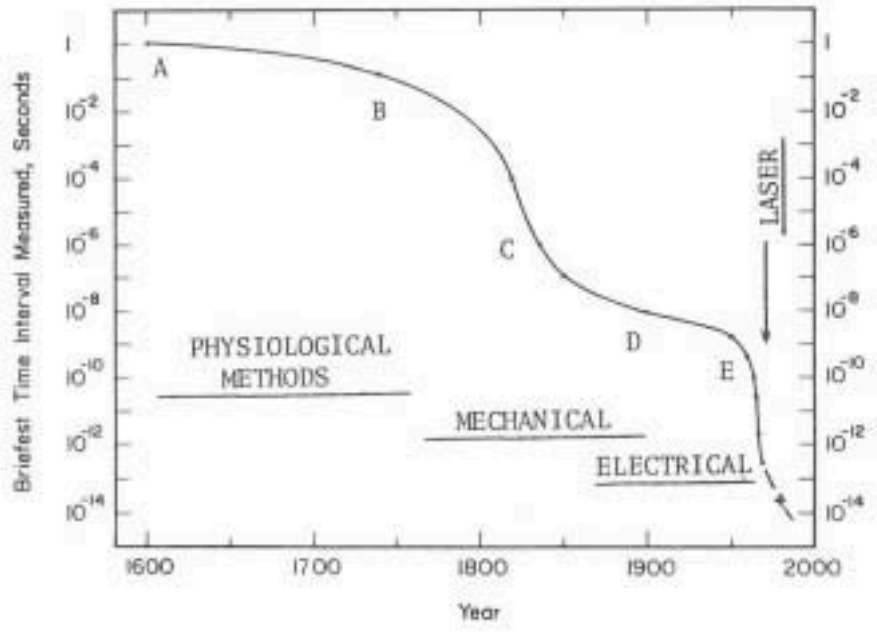

Fig.1. Progress in measurement of brief time intervals (after Shapiro [1]). A : Galilei (1580)- pulse timing, 1 sec resolution; B : Von Segner (1740) - image persistence on retina, 0.15 sec; C : Wheatstone (1834) - streaked image of spark by rotating mirror, 10^{-6} sec; D : Abraham (1899) - d.c. Kerr shutter 10^{-8} sec; E : DeMaria (1966) - modelocked Nd:glass laser, 10^{-11} sec.

2. Ultrashort Optical Pulse Generation

The progress in ultrashort light pulse generation is illustrated in Fig.2. Picosecond optical pulses were first generated by passively modelocked solid-state lasers [6,7]. Nd:glass lasers can easily be designed to provide pulses less than 10 psec in duration. Their major shortcomings are low repetition rate, due to thermal problems of the active medium, and output fluctuations. The flashlamp-pumped dye laser produces pulses 1.5 to 5 psec covering a broad range of wavelengths [8-10]. Being a flashlamp-pumped system, however, it still subjects to fluctuation and low repetition problems. Continuously-pumped passively modelocked dye lasers have generated the shortest optical pulses. The first laser of this kind by Ippen et al. [11] produced pulses as short as 1.5 psec. That system was later improved to generate pulsewidths ~0.3 psec [2]. With the colliding-pulse-modelocked (CPM) ring configuration, the cw dye laser has recently generated pulses shorter than 0.1 psec [3]. Self-phase modulation in an optical fiber followed by compression with a grating pair have shortened the durations of these pulses to approximately 30 psec [12].

The basic features of mode-locking can be understood from a simple analysis in the frequency domain. For each transverse mode of a laser resonator, there corresponds a set of longitudinal modes separated in frequency by $\delta\nu = c/2nL$, where c is the speed of light, L is the resonator length and n is the effective refractive index of the medium between the mirrors. Fig.3 shows typical spectrum of a laser, such as that of a HeNe laser measured with a scanning Fabry Perot interferometer. These are resonator modes with enough gain to overcome losses. The total field of the laser output is a sum of the oscillating modes :

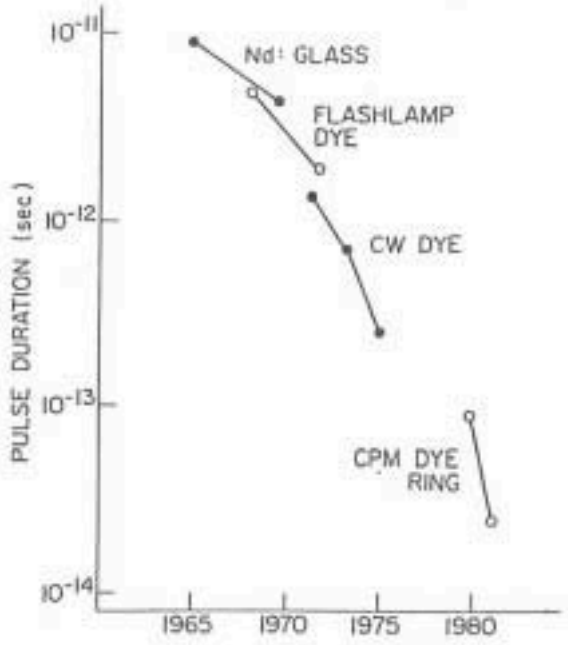

Fig.2. Progress in ultrashort optical pulse generation (after [5]).

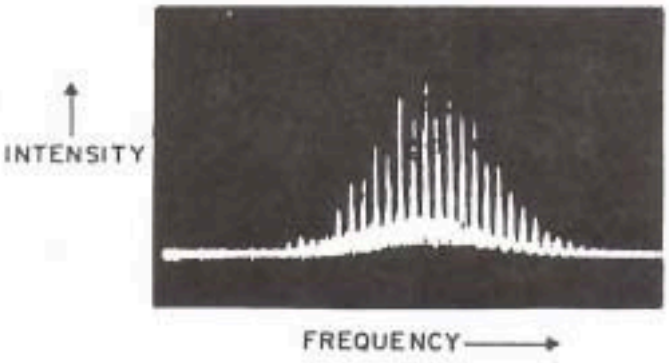

Fig.3. Typical spectrum of a laser.

$$E(t) = \sum_m E_m \exp\{i[2\pi(\nu_o + m\delta\nu)t + \phi_m(t)]\} \qquad (1)$$

where ν_o is an arbitrarily chosen reference frequency, E_m, ϕ_m are amplitude and phase, respectively, of the mth mode. In general ϕ_m's vary randomly with time, causing output intensity to fluctuate. Mode-locking occurs when the different modes are locked together in phase. Assuming all phases ϕ_m equal to zero, and that there are N oscillating modes with equal amplitudes E_o, the output intensity I(t) becomes

$$I(t) = |E(t)|^2 = E_o^2\left[\frac{\sin^2(N2\pi\delta\nu t/2)}{\sin^2(2\pi\delta\nu t/2)}\right] \qquad (2)$$

A plot of the square root of I(t), for N=5, E_o=1 is shown in Fig.4. Some properties of mode-locking are apparent : the output contains a train of pulses separated one from the other by T=2nL/c, with peak power equals to N times the average power, and individual pulsewidth t_p=T/N=1/$\Delta\nu$, where $\Delta\nu$ is the spectral linewidth of the laser. The modelocked pulse duration is thus, theoretically, inversely proportional to the laser bandwidth. Table I gives the bandwidths of some of the lasers most commonly used in mode-locking and the Fourier transform-limited pulsewidths. Actual pulse duration achieved depends on the method of mode-locking and properties of the material used. Incomplete locking of modes leads to pulses wider than the theoretical expectation.

There are two categories of mode-locking techniques : active and passive. Here we choose to describe only passively modelocked systems because they produce the shortest pulses. In passive mode-locking, a saturable absorber, whose transmission increases with light intensity, such as shown in Fig.5, is inserted into the optical path between the mirrors of the resonator. The resonator modes with random phases will not survive due to high losses at

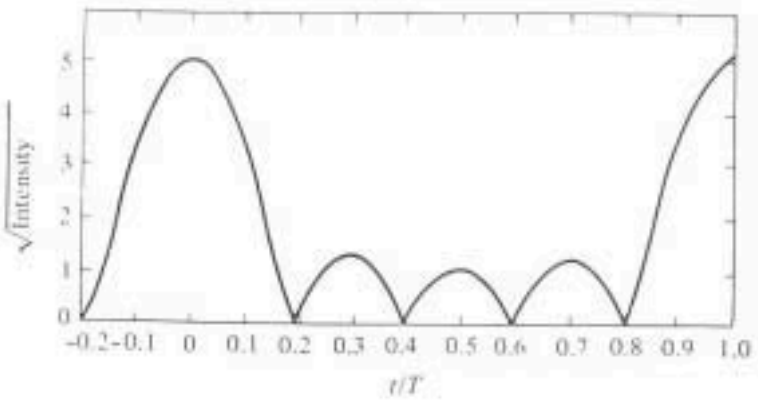

Fig.4. Theoretical plot of √Intensity versus t/T, where T=2nL/c is the round-trip time of light propagation in the resonator (after [13]).

Table 1. Bandwidths and Potential Pulsewidths of Some Commonly Modelocked Lasers

Laser Medium	Typical Bandwidth $\Delta\nu$ (Hz)	Transform-Limited Pulsewidth t_p (psec)
HeNe	1.5×10^9	600
Argon Ion	5×10^9	200
Nd:YAG	3×10^{10}	30
Ruby	6×10^{10}	15
Nd:Glass	3×10^{12}	0.3
Semiconductor	1×10^{13}	0.1
Dye	3×10^{13}	0.03

low intensities. The situation is different for those modes in phase with each other to form a pulse train according to Eq.(2), which are transmitted with slight attenuation due to the higher intensities of the pulses. Thus the insertion of the saturable absorber "forces" the laser to "lock" its modes through this "survival of the fittest" process.

The first picosecond optical pulses were obtained by modelocked solid-state lasers. A carefully-designed Nd:glass system typically produces pulses 5-8 psec in duration. Major disadvantages of the Nd:glass system are low repetition and fluctuation of pulse characteristics. Pulse energies and duration vary greatly from shot to shot. Even within the same train, pulse properties vary a lot according to its position in the train. However, with a before-amplification peak power typically $\sim$1 GW, the neodymium laser remains a powerful tool in the study of nonlinear processes where power is important.

Fig.6. depicts a typical neodymium system : the one we are using at National Central University in the study of hot electron phenomena in semiconductors. It uses a 5" long Hoya LHG-8 Nd-doped phosphate glass rod as

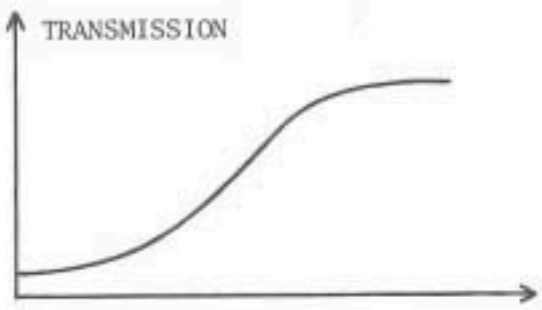

Fig.5. Transmission vs intensity in a saturable absorber.

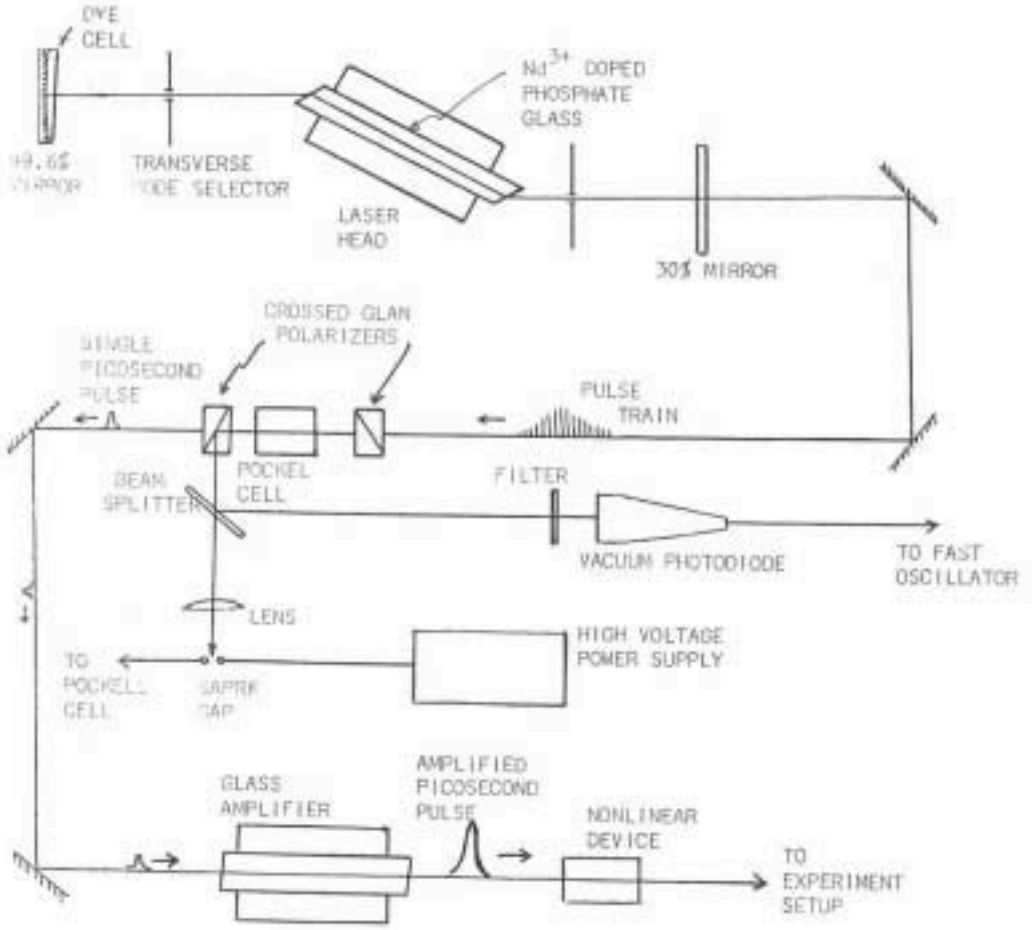

Fig.6. A modelocked Nd:glass laser system for picosecond studies.

oscillator medium and a 9" rod in the amplifier. Phosphate glass is chosen mainly for its low nonlinear refractive index n_2 (about 1.02×10^{-13} esu), such that glass damage due to self-focusing can be avoided. Besides, the relatively large cross-section for stimulated emission (about 4.2×10^{-20} cm^2) of this glass is also attractive. The laser is modelocked by flowing a 10:1 solution of dichloroethane and Eastman Kodak Q-switch dye A9860 through a cell in contact with the rear mirror. Operating at low repetition (below 6 ppm) and near threshold, it produces mJ pulses at 1.054μm, in a TEM_{00} low divergence ($\leq$ 1 mrad) beam. The mode-locked output from the oscillator consists of a train of about a hundred picosecond-pulses separated one from the other by approximately 10 nsec (Fig.7). To minimize fluctuation, a single pulse near the beginning of the train is switched out for our experiments. As shown in Fig.6, an electro-optical shutter is used in pulse selection. Laser beam deflected by the Glan polarizer illuminates a photodiode which, when power detected reaches a predetermined level, triggers a 6 nsec high voltage pulse which is applied to the Pockels cell to rotate light polarization by 90°, letting a single pulse to pass through the shutter. Typical pulse duration, measured by type II second harmonic generation in a nonlinear crystal (see next section), is about 8 psec. Other useful wavelengths can be generated by nonlinear optical methods : 5270Å, 3513Å and 2635Å, for example, are produced

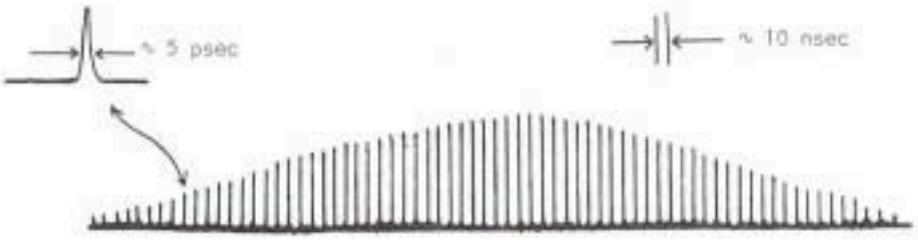

Fig.7. A modlocked pulse train.

by second, third and fourth harmonic generation, respectively. Recently, we have generated 0.85 - 1.4μm near infrared tunable output by optical parametric amplification in a temperature-tuned CDA crystal [14].

Passively mode-locked cw dye lasers have generated the shortest laser pulses. Fig.8 shows the system used by Ippen and Shank [2] to produce the first subpicosecond pulses. The gain medium, rhodamine 6G in a free-flowing stream of ethylene glycol, is located at a focal point approximately in the center of the resonator. The saturable absorber : a mixture of DODCI and malchite green dyes in ethylene glycol, another free-flowing stream, is located near one end of the resonator. Near the other end of the resonator is an acousto-optical cavity dumper that can dump optical pulses from the system at a rate up to 10^5 pps. This arrangement produces pulse energies that are at least an order of magnitude higher than that obtained from conventional output scheme with a partially transmitting mirror. In addition, this lower repetition rate is needed in many experiments to allow for complete sample

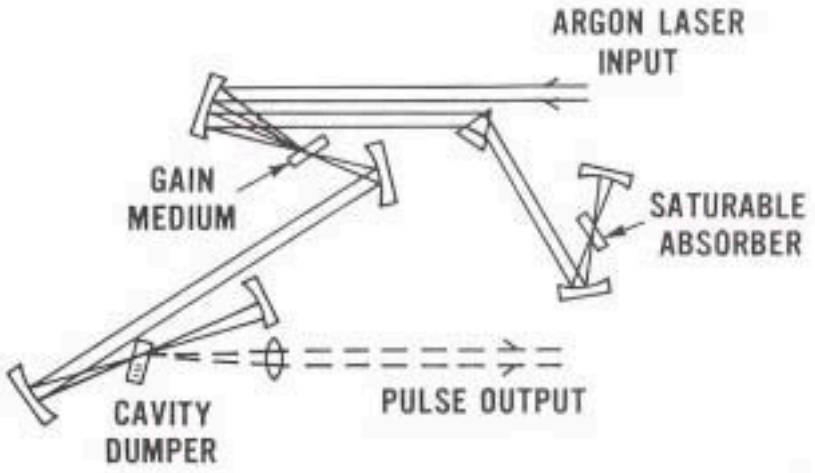

Fig.8. Cavity-dumped, passively modelocked cw dye laser (after [2]).

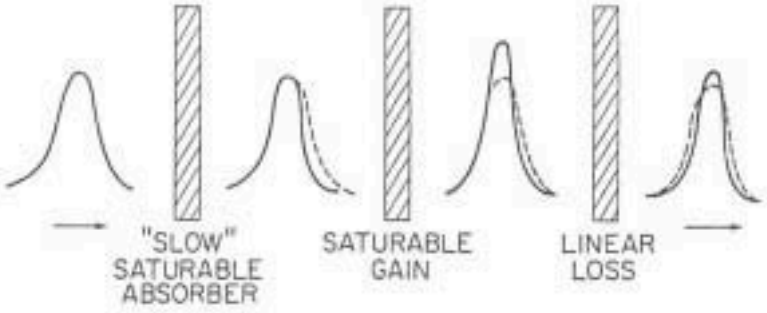

Fig.9. Pulse compression on passage through a slow saturable absorber, saturable gain, and linear losses of the system.

recovery between pulses. Subpicosecond optical pulses have been generated, with this system, at 615nm, with $\sim 5 \times 10^{-9}$J single pulse energy, equivalent to ~5kW peak power.

Measurements on DODCI has revealed a slow recovery time about 1.2 nsec [15]. This is in sharp contrast with the fast recovery (< pulsewidth) saturable absorbers used in mode-locking solid-state lasers. Here, in the absence of a fast absorber dye recovery, it is the combined effect of gain and absorber saturation that act to produce short pulses. With a slow recovery, the saturable absorber increases in transmittance during the passage of a pulse. As a result, the front portion of the pulse is attenuated more than the back portion. During passage through the gain medium, however, the back portion receives less amplification than the front due to gain saturation. On completing an oscillation, other resonator losses reduce the pulse energy to its original value. This pulse shortening process is illustrated in Fig.9.

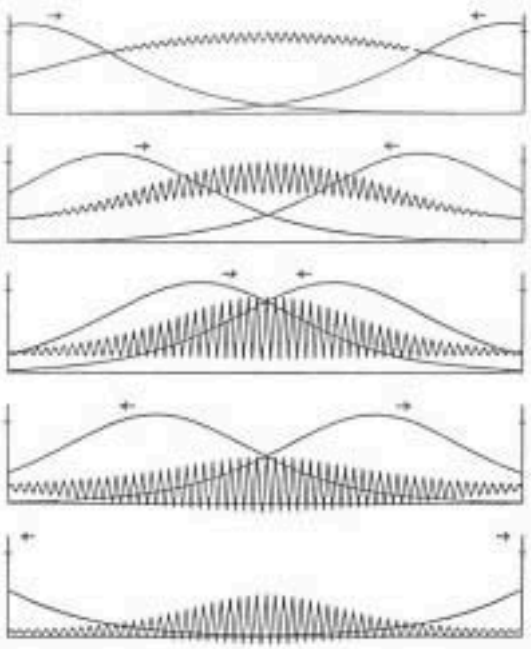

Fig.10. Bleaching and generation of an absorption grating in a saturable absorber by a pair of colliding optical pulses. Time sequence from top to bottom (after[5]).

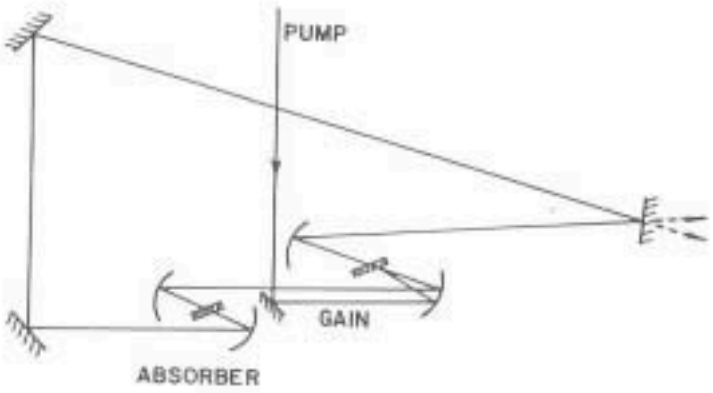

Fig.11. Schemetic diagram of a CPM ring dye laser (after [3]).

The first optical pulses shorter than 0.1 psec were generated by a colliding-pulse mode-locked (CPM) ring dye laser. In this laser, counterpropagating pulses "collide" in the saturable absorber, interfering to create a transient grating, as illustrated in Fig.10, in the population of absorber molecules, which in turn coherently scatters light from one pulse to the other. The mode-locking dynamics are similar to those of conventional cw dye lasers with slow absorbers, except here generation of the transient absorption grating tend to synchronize, stabilize, and shortens the pulses in a surprisingly effective way [3]. Schronization of the two counterpropagating pulses occurs because the minimum energy is lost to the absorber when the two pulses meet in the thin absorber stream. Quantitative analysis has shown that coherent coupling between the colliding pulses has a pulse shortening effect similar to an increase of the effective absorber cross-section [5,16]. The principal requirements for CPM are that the difference in arrival time of the two pulses be small compared to the pulse duration, and that the optical path in the absorber be equal to or less than the pulse duration. The first CPM laser is schemetically shown in Fig.11. The rhodamine 6G dye laser is pumped with a 3-7W cw argon ion laser at 5145Å. The free-flowing saturable absorber stream (3,3'-Diethyloxadicarbocyanine iodide dissolved in ethylene glycol) is approximately 10μm in thickness. The gain dye stream is so located that the counterpropagating pulses arrive at well-separated times. The focussing mirrors for the gain region have a 10-cm radius and those for the absorber have a 5 cm radius. The optical pulse duration has been measured to be about 90 fsec.

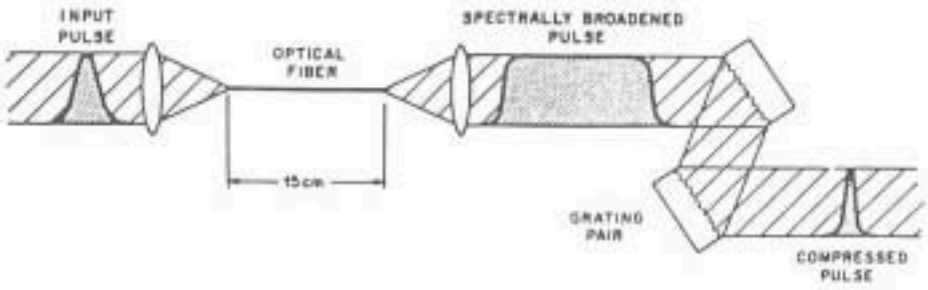

Fig.12. Experimental arrangement for short pulse compression (after [17]).

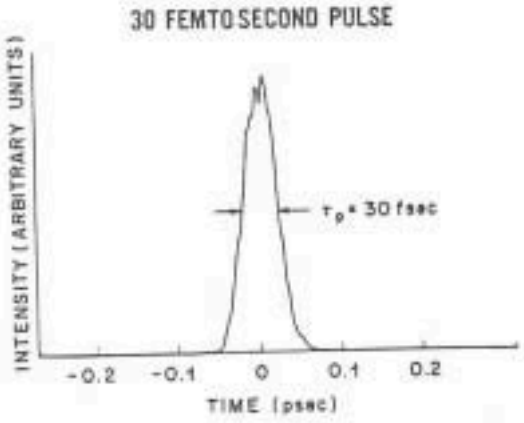

Fig.13. Result of an autocorrelation measurement on a 30 fsec pulse (after [17]).

Shorter CPM laser pulsewidths have been reported by Shank et al.[17] and Halbout and Tang [18].

Femtosecond pulses generated by a CPM dye laser have been further compressed to even shorter pulses. This is done with an arrangement shown in Fig.12. The femtosecond pulse is first focused into a short length of single mode optical fiber, in which self phase modulation causes a frequency chirping with lower frequencies leading higher frequencies. The chirped pulse, without a change in shape, may be compressed by passage through an anomalously dispersive medium. This is accomplished by having the spectrally broadened pulse pass through a matched grating pair, as shown in Fig.12, a method originally devised by Treacy [19-21]. The compressed pulse has a duration of 30 fsec,

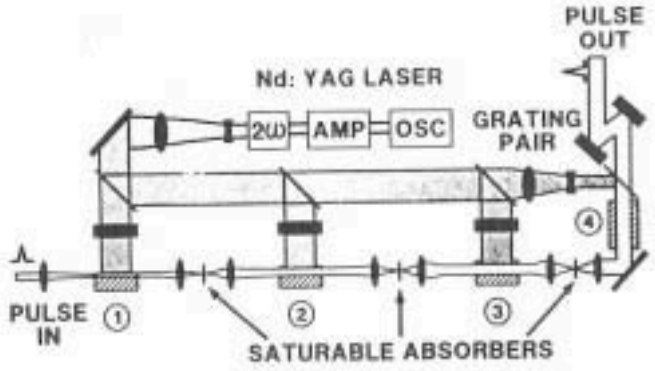

Fig.14. A 4-stage femtosecond optical pulse amplifier (after [17]).

the shortest optical pulse reported today. Fig.13 shows the result of an autocorrelation measurement (see next section on pulsewidth measurement techniques) on this pulse.

The relatively low intensities (typically 1-10 kW peak power) of dye lasers pose a problem in experiments where more intense pulses are essential. It is thus often necessary to amplify dye laser pulses to the required power levels. A system used by Shank et al. [17] to amplify their femtosecond pulses to energy levels in excess of a gigawatt is depicted in Fig.14. It has four dye amplifier stages, three transversely pumped, one longitudinally

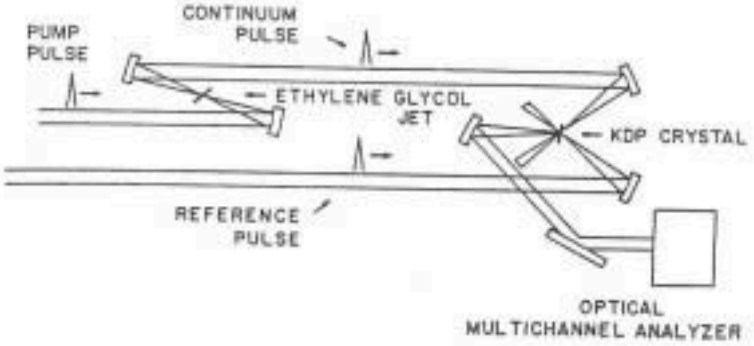

Fig.15. Femtosecond continuum generation and measurement (after [26]).

pumped by pulses splitted off, at successively larger fractions, from a frequency-doubled Q-switched Nd:YAG laser pulse. Single subpicosecond pulses from a CPM dye laser are selected in synchronism, with a timing jitter less than 1 nsec, with the pump pulses to ensure gain optimization. Beam diameter is expanded appropriately between stages. Streams of saturable absorber malchite green are used to isolate the stages from each other, to suppress amplified spontaneous emission, and to reshape the amplified pulses. An incident 90 fsec pulse is broadened to about 400 fsec during passage in the dispersive

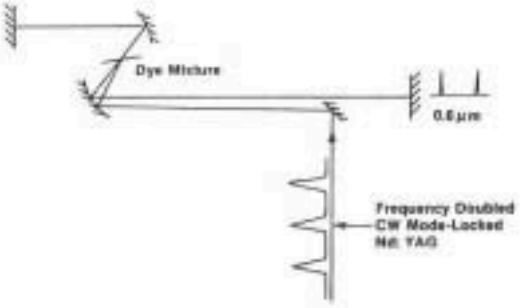

Fig.16. Generation of pulses shorter than 70 fsec with a synchronously-pumped cw dye laser (after [4]).

amplifiers. A grating pair is used after the final amplifier stage to compress the chirped pulses. The pulse is restored to 70-90 fsec duration with a peak power at gigawatt levels [17,22].

For high speed time-resolved spectroscopic measurements, white light continuum picosecond and subpicosecond pulses are extremely useful. They enable one to measure, for example, the entire absorption spectrum of a sample in a single shot. A continuum can be generated by focusing an intense pulse into a nonlinear medium such as glass, calcite, quartz, H_2O, D_2O and CCl_4 [23-25]. Fig.15 shows an experimental arrangement which Fork et al.[26] uses in femtosecond continuum generation. A pump pulse at 627 nm of 65 fsec duration, generated by a CPM dye laser and amplified by a 4-stage Nd:YAG pumped dye amplifier system to 1.2 GW peak power, is focused into a 500 μm thick jet of ethylene glycol. The recollimated pulse, and a delayed reference pulse splitted off from the pump, are focused at a thin (100μm) KDP crystal. Upconverted light is observed with an optical multichannel analyzer. Cross-correlation functions are obtained by varying the optical path of the reference pulse. The continuum pulse generated is measured to have a broad

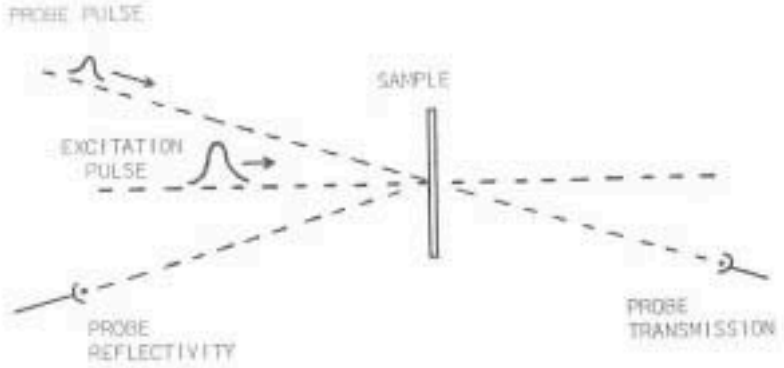

Fig.17. Excite-and-probe experiment.

spectral range of 0.19-1.6μm, with a pulsewidth of about 80 fsec, and a peak power about 1 GW.

As a last comment, optical pulses shorter than 0.1 psec have been generated by methods other than CPM. As an example, Fig.16 shows schemetically a synchronously-pumped cw dye laser system that generates femtosecond optical pulses [4]. The gain dye : rhodamine 6G and the fast recovery saturable absorber : DQOCI are mixed in a solution of ethylene glycol. The

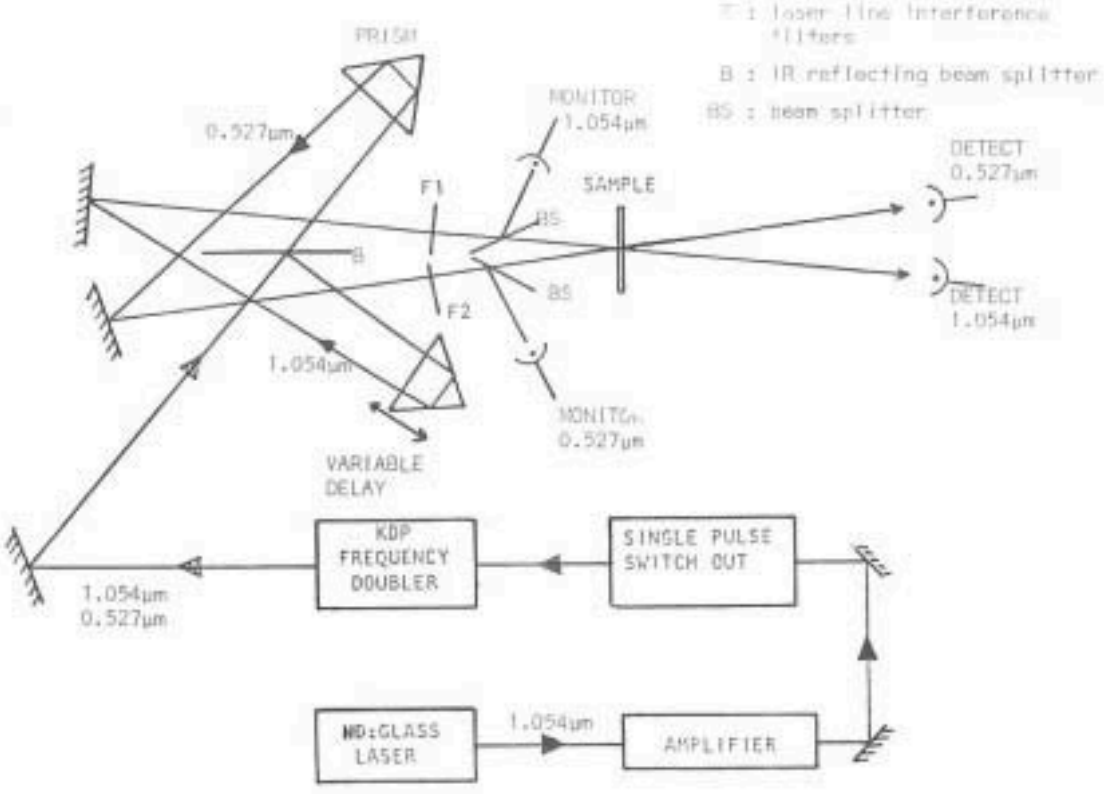

Fig.18. An excite-and-probe setup for measuring excitation dependence of free-carrier absorption in semiconductors.

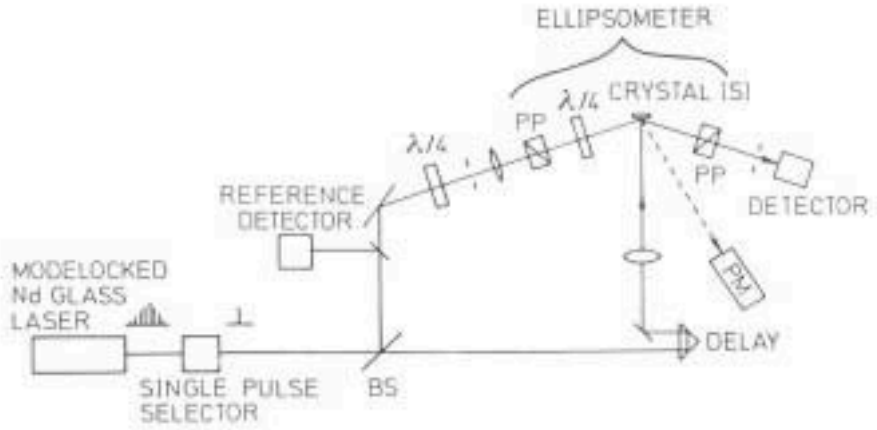

Fig.19a. A picosecond ellipsometer used to measure photo-induced refractive index change in a semiconductor (after [28]).

dye mixture jet (200μm thick) is synchronously pumped by a frequency-doubled cw mode-locked Nd:YAG laser of matched cavity length. The laser is tunable over 590-615nm. Pulsewidth measurements using a background-free autocorrelator indicate that the shortest pulsewidth : 70 fsec, is obtained at 615nm where the laser exhibits a maximum stability and maximum output power, reflecting the dramatic effect of the saturable absorber, For a 300 mW average pump power, the output is 30 mW. The large laser spectrum (120Å) and evidence of frequency chirp observed indicate that pulses as short as 30 fsec may be

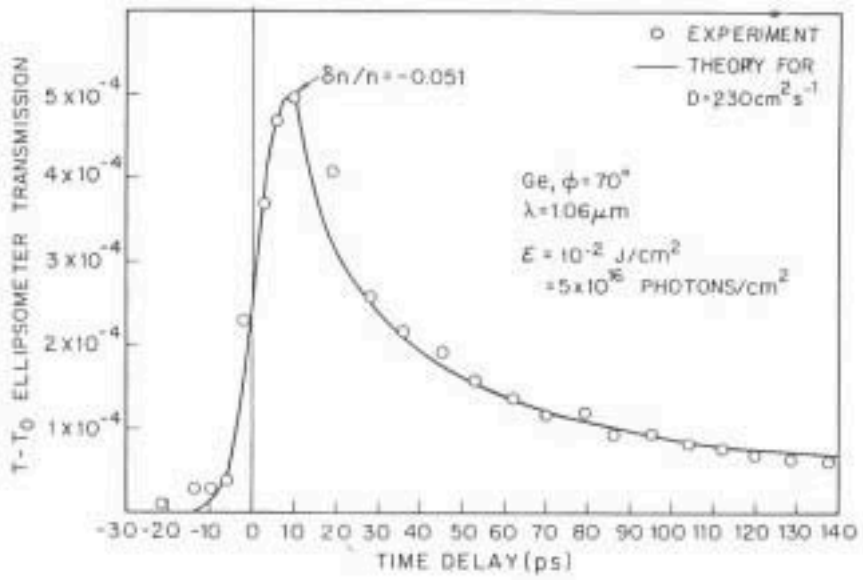

Fig.19b. Ellipsometer transmission vs time delay. The solid line is a theoretical fit using an ambipolar diffusion model, with effective diffusion constant D (after [28]).

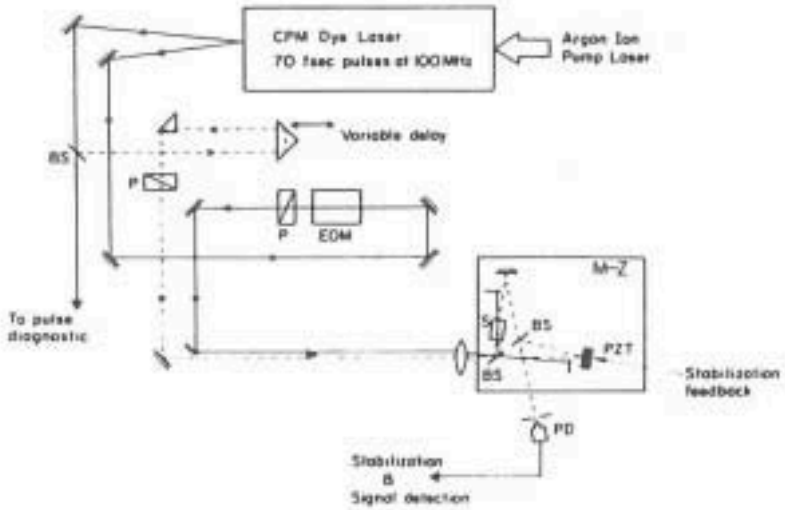

Fig.20a. A femtosecond interferometer for nonlinear optics studies. BS: beam splitter, EOM: electrooptic modulator, M-Z: Mach-Zehnder interferometer, P: polarizer, PD: photodetector, S: sample cell (after [18]).

obtained with the use of a grating pair pulse compressor, and the design of a dispersion-free cavity. With this setup, the pump pulses and the generated pulses can easily be synchronized to a picosecond accuracy. Therefore, efficient amplification of the pulse energy to the mJ level with a synchronously pumped dye amplifier system can readily be achieved.

3. Measurement Techniques

The availability of ultrashort optical pulses has provided scientists an extremely useful tool for direct measurements of ultra-high speed phenomena. Numerous experiments, in all major areas of science : physics, chemistry, biology and engineering, have been performed since the first appearance of modelocked lasers more than 17 years ago. Major methods of measurement are described in this section. The powerfulness of these techniques are illustrated with a number of representative examples.

3.1 Excite-and-Probe Techniques

The modelocked laser pulse, with its extremely high peak power, can easily create a highly excited region in a sample. The state of the medium can then be probed with another short pulse (Fig.17). Splitted-off from the same modelocked pulse as the excitation, the probe is allowed to pass through

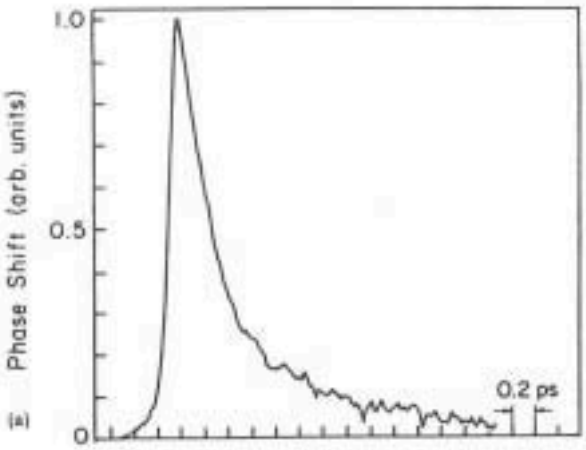

Fig.20b. Photo-induced phase shift in a CS_2 cell as a function of time delay between excitation and probe (after [18]).

a variable optical delay path. By varying the delay of the probe pulse, transient phenomena in the excited medium can be investigated, with a time resolution equal to the pulse duration, as a function of time after excitation. To avoid significant perturbation of the state of the excited medium, the probe is generally much weaker than the excitation. Since the entire integrated pulse energy is monitored, no high detector or electronics is needed.

The excite-and-probe method has been applied to studies of photo-induced transparency, absorption, refractive index change, birefringence and other phenomena in a medium. It is the most widely-used technique for ultrafast measurements. In fact, the first picosecond measurement with optical pulses

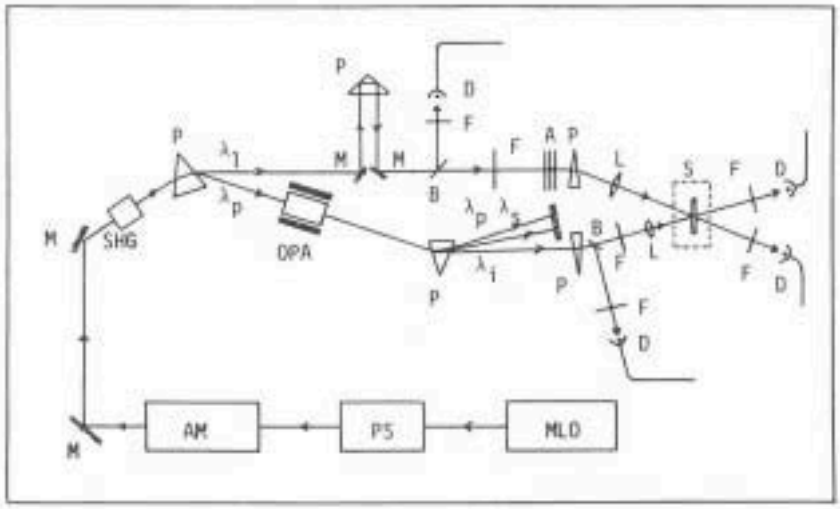

Fig.21. A frequency-doubled Nd:glass laser-pumped optical parametric amplifier (OPA) system for excite-and-probe studies. PS: pulse selector, AM: amplifier, M: mirror, P: prism, L: lens, D: detector, B: beam splitter, A: attenuator, F: narrow band filter, S: sample. Laser, pump, signal and idler wavelengths are indicated by λ_1, λ_p, λ_s and λ_i, respectively.

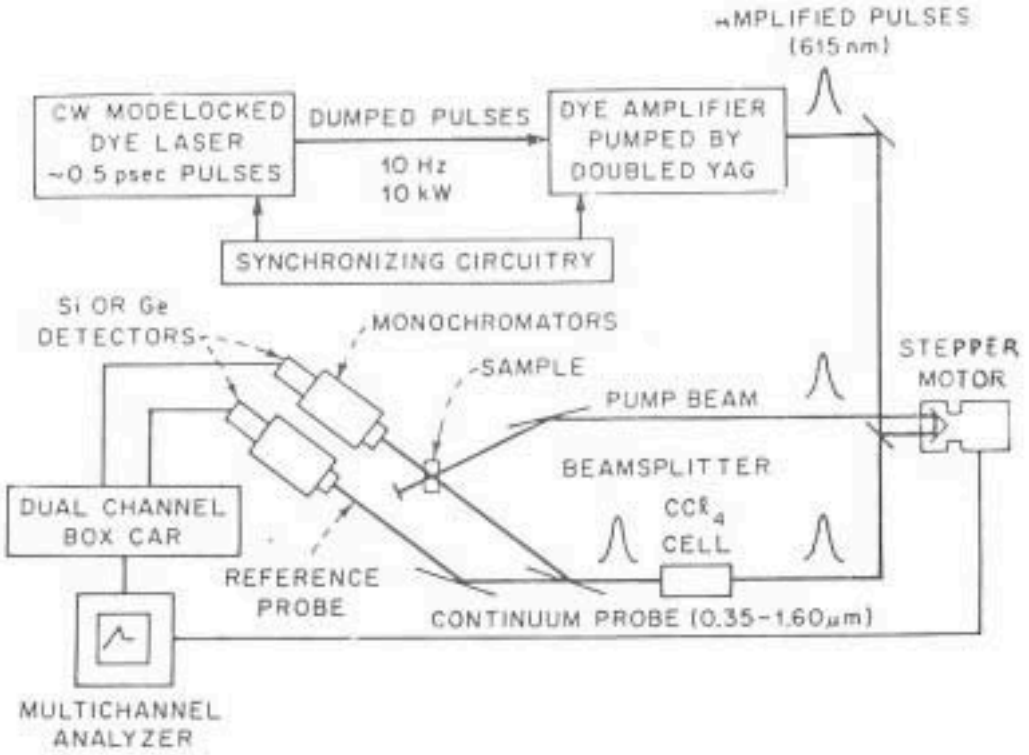

Fig.22. Experimental arrangement for picosecond continuum spectroscopy (after [36]).

was an excite-and-probe experiment [27]. Shelton and Armstrong used their laser to saturate the absorption of a Q-switching dye. Absorption recovery was then monitored by delayed pulses. The entire pulse train was used in both excitation and probe in this early experiment.

Fig.18 illustrates a typical experiment in which the transmission of a sample is measured. We have used this setup to study excitation dependence of free-carrier absorption in semiconductors. A single pulse, selected from a modelocked Nd:glass laser and upconverted to $2h\nu$ photon energy in a KDP second harmonic generator, is used to excite a semiconductor whose bandgap E_g is such that $h\nu < E_g < 2h\nu$. The excitation pulse is entirely absorbed, via direct interband transition, creating a dense electron-hole plasma at the interaction spot. The unconverted portion of the pulse is used to probe the excited medium. With photon energy less than bandgap, this pulse is absorbed by intraband transitions. A measurement of probe transmission thus reveals density and state of the free-carriers. Experiments have been performed on GaAs, CdTe and InP.

An example where measurement is made on the reflectivity is shown in Fig. 19a. In this particular experiment, photo-induced refractive index change is measured with an ellipsometer which monitors the change in ellipticity of light reflected from the sample surface [28]. Purpose of the experiment is to investigate the transient behavior of a photo-generated electron-hole plasma in a semiconductor. A single pulse selected from a modelocked Nd:glass

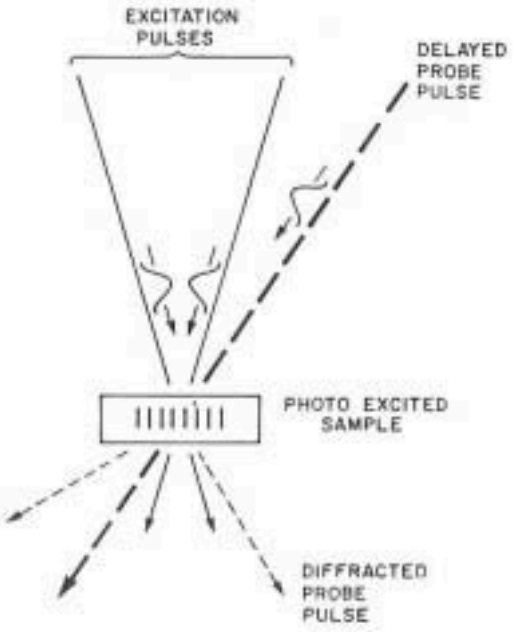

Fig.23. Probing of laser-induced transient grating (after [37]).

laser pulse train is splitted by a beam splitter into two parts. The strong part is used to excite the sample, which is a piece of intrinsic Ge crystal. A dense electron-hole plasma is created, by direct interband transitions, at the interaction spot. As a result, there is a slight change in refractive index. The plasma is intially confined, due to high absorption, in a layer about 1 micron within the irradiated surface. It rapidly diffuses into the bulk after its creation. The diffusion rate can be measured by monitoring refractive index change, as a function of time after excitation, with the weak part of the splitted pulse which passes through the ellipsometer as shown. Polarizers of the ellipsometer are set such that no light passes through when excitation is blocked. Then the transmission through the ellipsometer is $\Delta T \propto |\delta n/n|^2$, where n is the index of refraction and δn is the index change. Incident energy is monitored shot by shot with a reference detector. Each data point in Fig.19b is an average of 10 shots. Peak ellipsometer transmission of 5×10^{-4} corresponds to a negative index change $\delta n/n = -0.051$. The solid line is a theoretical curve according to the ambipolar diffusion model. Free-carrier density is estimated to be about 1.7×10^{20} cm^{-3}. The diffusion constant $D = 230$ cm^2/sec obtained is much higher than the known constant of 65 cm^2/sec obtained from low carrier density measurements. This diffusivity increase can be accounted for with a degenerate electron-hole plasma model.

Induced changes in index of refraction has also been measured by an interferometer method. An arrangement which Halbout and Tang [18] have used in the study of third order nonlinearity in CS_2 is depicted in Fig.20a. The laser used is a colliding-pulse modelocked (CPM) rhodamine 6G ring dye laser emitting in two beams highly stable 70fsec long pulses, at 619.5 nm wavelength, at a repetition rate of 100 MHz. For a

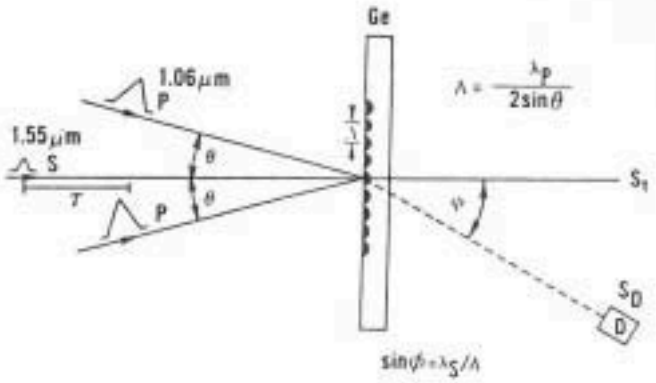

Fig.24. Measurement of diffusion and recombination effects in a semiconductor by diffraction from an optically-induced picosecond transient grating.

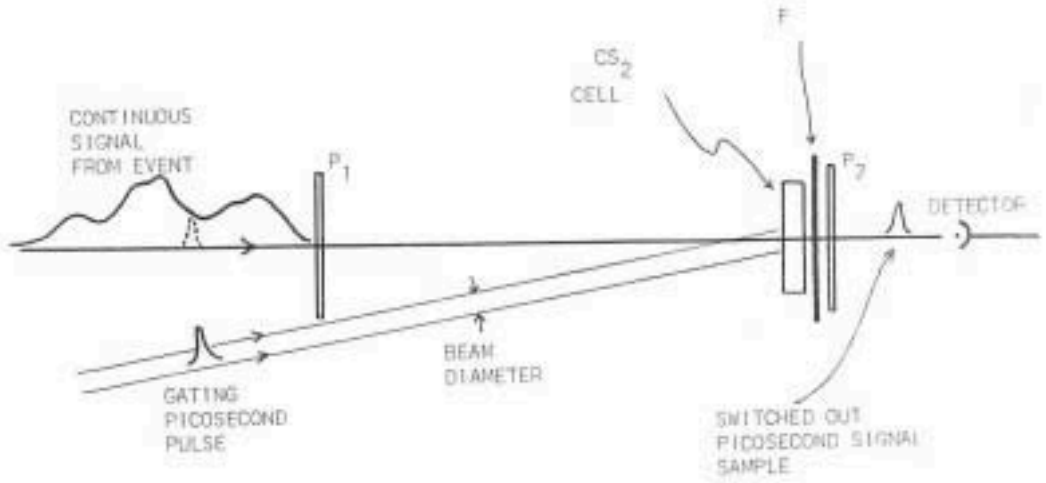

Fig.25. The ultrafst optical shutter.

pump power of 5-6W from an argon ion laser, output power in each beam is 30mW. The strong excitation and the weak probe, derived from the two output beams as shown, overlap both spatially and temporally in a 1-cm CS_2 cell which is placed in one arm of an actively stabilized Mach-Zehnder interferometer. The strong excitation introduces, via third-order nonlinear refractive index, a phase shift between the two arms of the interferometer. This phase change is observed by the probe beam as a function of the time delay between excitation and probe. The excitation beam is amplitude modulated at 1 kHz by an electro-optic modulator to avoid the interferometer being perturbed by a spurious component at signal frequency. Feedback stabilization of the interferometer is

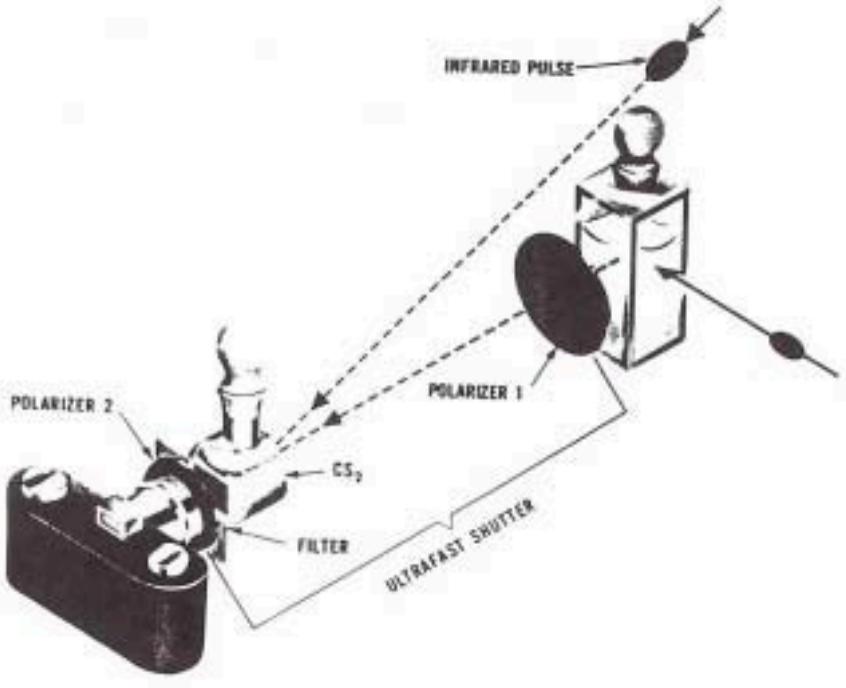

Fig.26. Experimental arrangement for the photography of a light pulse in flight (after [40]).

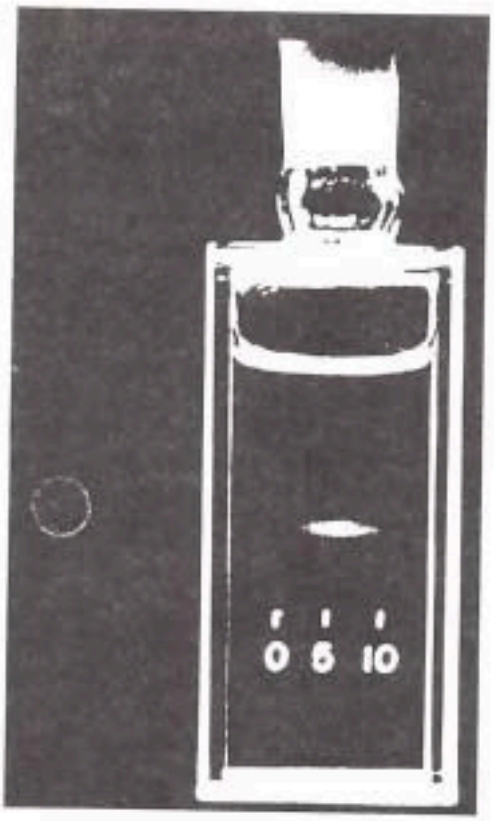

Fig.27. A picosecond optical pulse photographed "in flight" as it propagates from right to left through a cell of milky water. The scale is in millimeters. The shutter open time is about 10 psec.

achieved by synchronous detection at twice the modulation frequency followed by an integrator and a high-voltage operational amplifier which drives the PZT. Only one detector is needed for both stabilization and signal detection. Data obtained is depicted in Fig.20b, which exhibits a double-exponential decay characteristic. Fitted to a function of the form : $A\exp(-t/T_1) + B\exp(-t/T_2)$, the best fit is obtained with A=0.86, B=0.14, T_1=0.36 psec, T_2=2.07 psec. There are two intrinsic contributions to the third order nonlinearity. First, a "purely electronic" contribution arising from nonlinear distortion of the electronic distribution around a fixed nuclear configuration of the molecules. Second, a contribution of "nuclear" origin due to optical field-induced nuclear motion of the molecules which indirectly affects electronic polarizability. Since the purely electronic contribution should not extend beyond the width of the cross-correlation between the two beams, experimental result thus confirms that the prodominant contribution to the third-order nonlinearity in CS_2, down to subpicosecond regime, is of

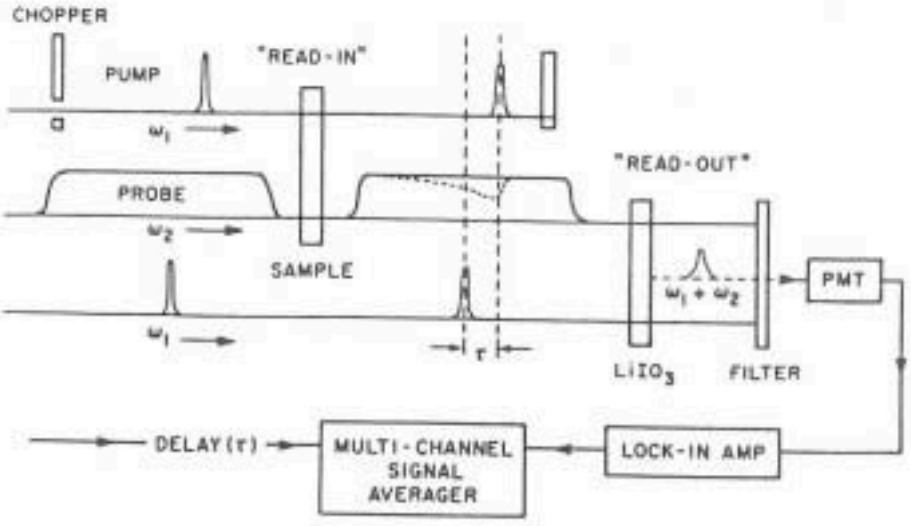

Fig.28. "Read-in" -"read-out" measurement by optical gating (after [47]).

nuclear origin. This interferometry technique can readily be extended to the study of other materials including solids.

Passively modelocked cw dye lasers, such as the one used in the above example, featuring subpicosecond pulsewidth, high repetition rate, excellent pulse stability and wavelength tunability, are ideal for ultrafast phenomena studies, particularly when small effects ar being measured. Operating at high repetition rates, powerful signal averaging methods can be applied to enhance signal/noise ratio. Recent improvements of pulse reproducibility with CPM systems have further improved detection sensitivity and signal-to-noise ratio. Recently, detectibility as low as 10^{-7} has been achieved in a sampling experiment [29].

Since both the excitation and the probe are derived from the same laser pulse, care must be taken in interpreting experimental data for delay times equal to or less than pulse duration. Here, coherent coupling between the two beams occurs. Spatial interference produces in the sample medium a periodic nonlinear polarization, which scatters the excitation beam into the probe beam. This effect has been observed in a number of experiments [15,30, 31].

In investigation of ultrafast processes, it is often needed to excite the sample at one wavelength and than probe it at another wavelength far apart in the spectrum. One convenient approach is the use of nonlinear optical devices. Nonlinear crystal parametric amplifiers (OPA) are particularly useful in the generation of short pulses in the infrared. A system using $LiNbO_3$ crystal (Laubereau et al. [32]), for example, may be tuned between 1.4 and 4μm. This wide tuning range has find useful applications in the studies of the vibrational dynamics of polyatomic molecules. Fig.21

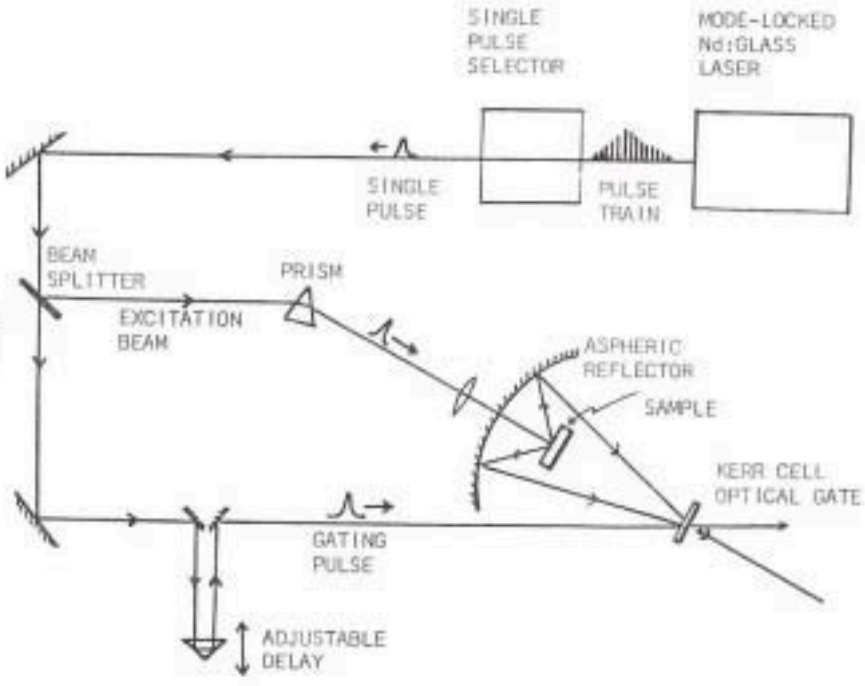

Fig.29. Optical gating setup for time-resolved observation of photoluminescence in semiconductors.

shows an optical parametric amplifier system which we have used in the study of the transient behaviors of photogenerated electron-hole plasmas in semiconductors [14]. Picosecond pulses at 1.054μm are selected from a passively modelocked neodymium-doped phosphate glass oscillator-amplifier laser system. Typical single pulse energies are 5-10 mJ. An angular phase-matched temperature-stabilized KDP crystal is used to generate, at a conversion efficiency > 30%, second harmonic wave at 0.527μm, which in turn pumps a 1.5 cm long temperature-tuned CDA crystal OPA. The CDA crystal is cut in the 45 degrees z-cut orientation, with the pump beam,polarized along the optic axis, propagates along the [110] direction. To avoid crystal damage, irradiance on the crystal is kept below 500 MW/cm^2 by careful control of beam diameter. Output from the OPA is tunable over the range 0.85-1.4μm by varying crystal temperature between 40 and 70°C [33]. Strongly dependent on pump power and output wavelengths, conversion efficient of the OPA varies from 0.1% to a few percent in our experiment. The unconverted 1.054μm pulse, goinh through a

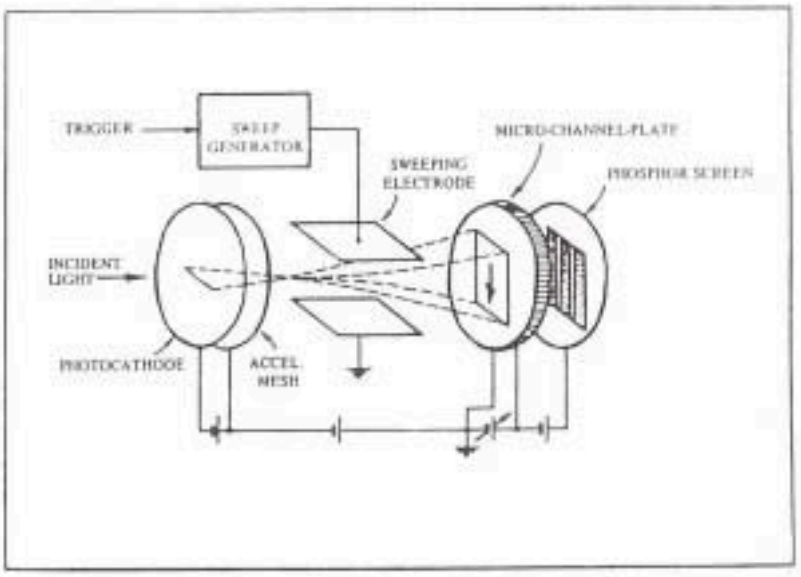

Fig.30. Operation of a streak tube.

variable delay path and a set of attenuators, is used to excite the sample. Probing of the interaction spot ultilizes converted pulses at different wavelengths.

Picosecond and subpicosecond continuum, generated by focusing a short pulse into a nonlinear medium in the manner described in the last section, enables researchers to record ultrafst response in a broad spectrum in a single shot [34]. As an example, Fig.22 shows an experiemntal arrangement used by Fork et al. [35,36] for picosecond continuum spectroscopy of amorphous and crystalline semiconductors. Subpicosecond pulses (0.5 psec) from a passively modelocked dye laser operating at 0.61 μm are cavity-dumped at 10 Hz rate. These pulses are amplified to 2 GW peak power in a dye amplifier system and divided into two beams. The first beam excites the sample after passing through a variable delay line. The second is focused into a cell containing H_2O or HCl_4 to generate a broad continuum from 0.35 to 1.6 μm. The subpicosecond continuum is used to probe the absorption of the pump-excited sample.

3.1.1 Laser-Induced Transient Grating Method

Coherent coupling between two beams in a medium, a source of artifact in excite-and-probe experiments when the delay time between the two pulses is shorter than pulsewidth, can be ultilized to measure ultrafast processes in the laser-induced transient grating method : a variation of the excite-probe technique. In this technique (Fig.23) the excitation is splitted into two pulses which spatially and temporally overlap in the sample. Interference between the two excitation beams results in a periodic intensity distribution which induces a photo-excited grating in the sample. This grating rapidly decays in time when the photo-excited state relaxes or diffuses away. A delayed probe pulse passing through the interaction spot at some angle is diffracted into different orders by the transient grating. Thus the decay mechanisms can be measured by monitoring the intensity of the diffracted light in one of the side orders. This method has the advantage that the measured signal is background free when only one side order is detected. In addition, spatial diffusion effects can be studied by varying the grating spacing, which is determined by the angle between the excitation beams. Phillion et al. used this technique to study the rotational relaxation of rhodamine 6G molecules in solution [37].

This technique has been used by Moss et al. [38] in a measurement of diffusion and recombination effects in germanium (Fig.24). The light source used is a Nd:YAG laser, operated in the TEM_{00} transverse mode, generating

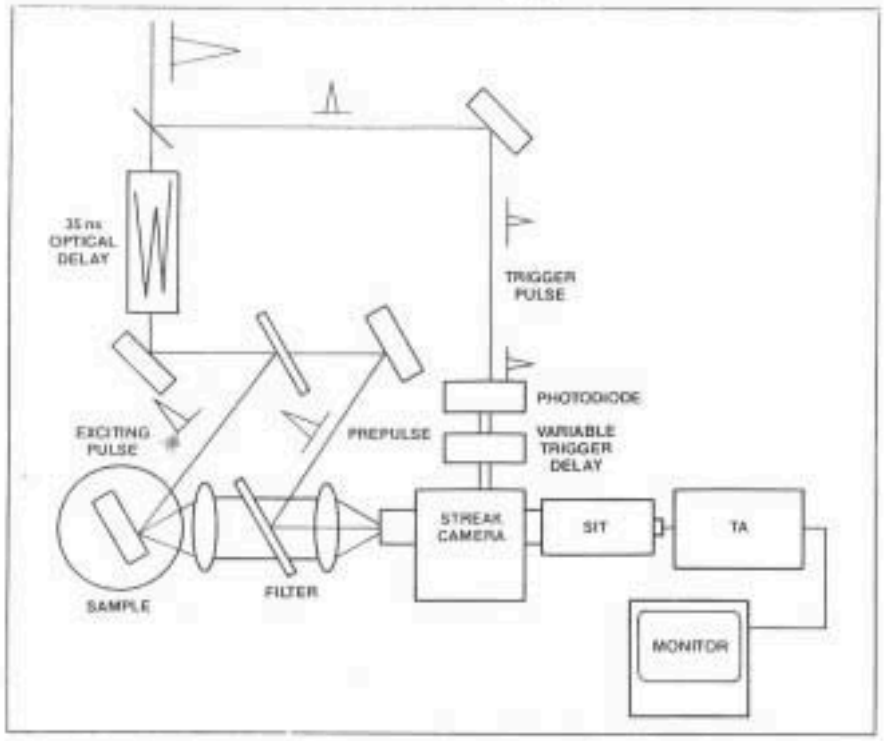

Fig.31. Experimental arrangement for time-resolved emission studies using a streak camera (after [50]).

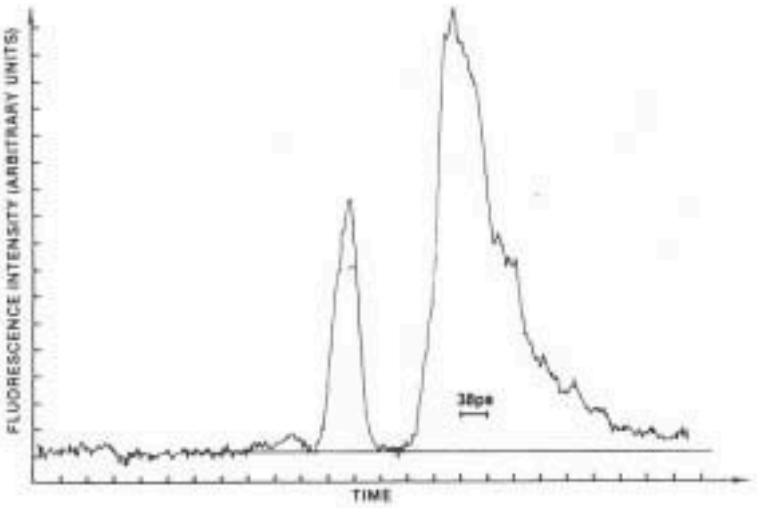

Fig.32. Fluorescence decay profile of erythrosin dye in water, recording with a streak camera. The first peak is a pre-pulse marker (after [50]).

35-psec pulses at 1.06μm. The excitation pulses are focused onto a 6-micron thick Ge sample. A spatially modulated carrier density is produced by direct absorption of the excitation pulses. Decay of the grating is monitored by measuring the first-order diffracted light from a probe pulse at 1.55μm as a function of time delay between excitation and probe. The probe pulse is generated from the 1.06μm pulse by stimulated Raman scattering in benzene. Since the photon energy of the probe is less than the direct bandgap of Ge, it interrogates principally an index grating. By measuring the lifetimes of gratings of different spacings (controlled by varying 2θ), and data fitting with a linear diffusion-recombination model, diffusion coefficient has been obtained along with an estimation that the bulk recombination lifetime is longer than 1 nsec.

3.2 Light Gating Methods

3.2.1 The Optical Kerr Shutter

The operation of an ultrafast optical shutter is illustrated in Fig.25. Originally, light from a fast transient event cannot pass through the shutter composed of a carbon disulfide cell situated between two crossed polarizers. When an intense, polarized ultrashort optical pulse (the gating pulse) traverses the CS_2 cell, it induces a short-lived birefringence due to orientation of the polar molecules. This "opens" the shutter, allowing light from an event to be transmitted for a brief interval (∿ duration of the gating pulse). By varying the delay of the gating pulse with respect to the event, different time-sections of the signal can be obtained. F in Fig.25 is a filter used to to block the gating pulse. This fast shutter was first proposed by Duguay and Hansen [39]. To demostrate its speed, they have used the setup in Fig.26 to photograph a light pulse in flight [40]. An infrared pulse from a mode-locked Nd:glass laser opens the Kerr shutter, which replaces the mechanical shutter of a camera, for about 10 psec. A green pulse, frequency-double from

the IR pulse, traverses a cell of milky water. Light scattering makes the pulse visible from the side, so that it can be "stop-motion" filmed in flight (Fig.27).

The Kerr shutter described above has been widely used in time-resolved light emission studies [41-43]. Compared to the optical gating by frequency-mixing technique described below, this method has the advantages of broadband frequency transmission and large angular acceptance. Time resolution of the gate is limited by both the gating pulsewidth and the Kerr lifetime. Orientation re-ramdomization time of CS_2 molecules has been measured to be about 2 psec [44]. Using subpicosecond gating pulses, resolution of the gate is thus Kerr response-limited. We have used the setup in Fig.29 in time-resolved observation of photoluminescence in semiconductors. The photo-excited sample is placed at one focus of an elliptical mirror while the Kerr shutter is positioned at the other focus. Part of the amplified 1.054μm picosecond optical pulse, selected from a passively modelocked Nd:glass laser, is used to open the shutter. Photoluminscence from the front surface is collected as shown. Strong excitation with picosecond pulses has enabled us to observe photoluminscence across the direct bandgap in Ge, which is an indirect gap semiconductor.

3.2.2 Gating by Nonlinear Optical Mixing

In this technique, the optical signal of interest is mixed with a picosecond or subpicosecond laser pulse in a nonlinear crystal for sum frequency

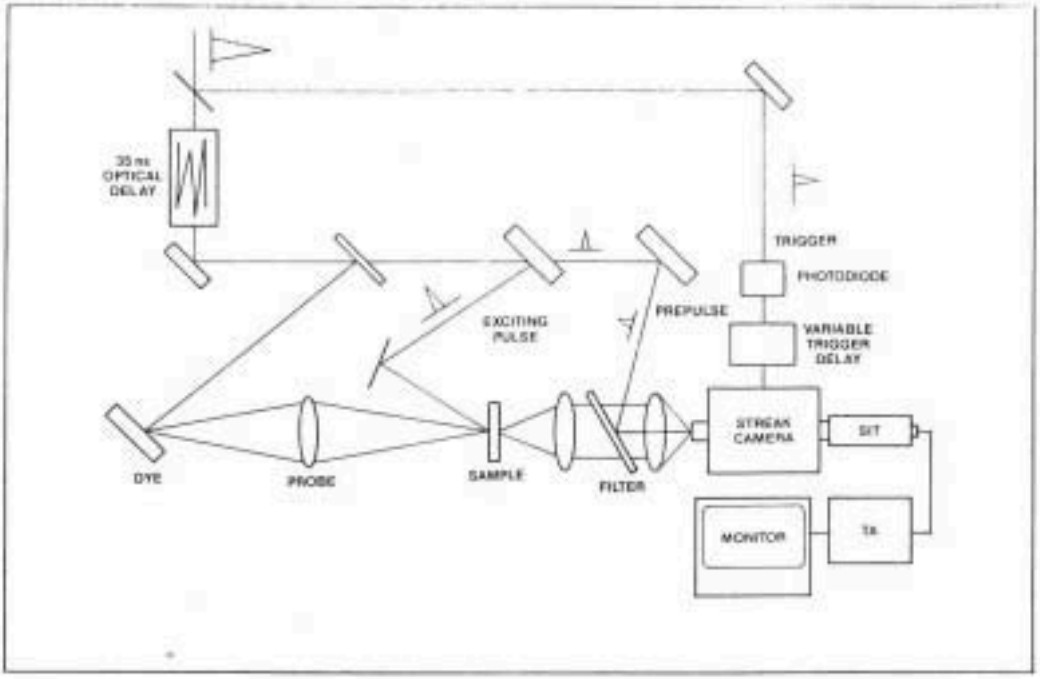

Fig.33. Transient absorption measurement using a streak camera (after [51]).

generation. In the first experiment reported by Mahr and Hirsch [45], luminescence was studied by mixing with picosecond dye laser pulses in a phase-matched ADP crystal. Up-converted signal which was in the uv was detected. The setup acted as an optical gate which was opened by the picosecond pulse. Strength of the up-converted light pulse was proportional to the signal power. Temporal behavior of the signal was obtained by measuring the converted power while the arrival time of the gating pulse was varied. Recently, this technique has been applied in the measurement of pulse delay in a single-mode optical fiber [46].

A "read-in" - "read-out" measurement scheme using optical gating is illustrated in Fig.28 [47,48]. A subpicoseond optical pulse train at ω_1 is divided into two beams. One beam, modulated by a chopper, excites a sample. A tunable cw or long pulse laser is used to probe the response of the excited sample at ω_2. The change in the probe is then monitored by optical mixing with the delayed part of the subpicosecond pulse train in a $LiIO_3$ crystal. With gating pulses at 615nm and probe wavelengths > 560nm, upconversion efficiency in the $LiIO_3$ crystal is typically about 10%. One advantage of this technique is its speed : temporal resolution is completely determined by the gating pulse. Also, detection is background-free since upconverted signal exists only in the presence of the gating pulse. However, for efficient conversion, accurate angular positioning of the nonlinear crystal is required for phase-matching between the mixing waves.

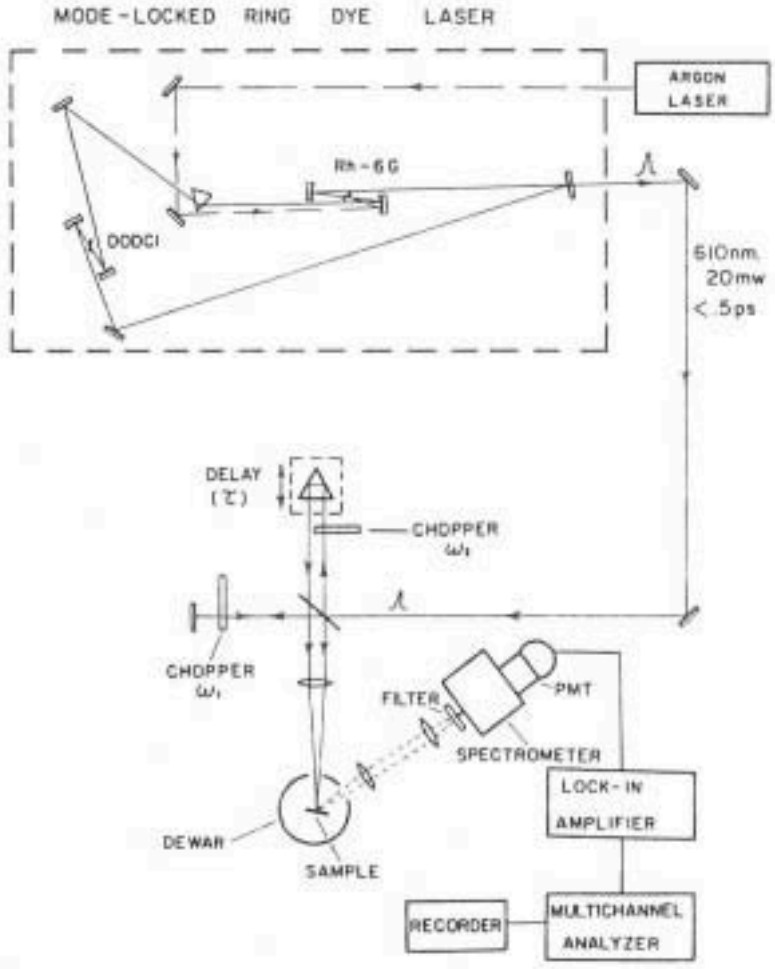

Fig.34. Time-resolved photoluminescence by the population-mixing technique (after [52]).

3.3 Measurements with a Streak Camera

Basic operation of a streak camera is illustrated in Fig.30. Light from a transient event strikes the photocathode, causing emissions of electrons in proportion to instantaneous light intensity. The electrons are then accelerated by an accelerating mesh and deflected by a voltage ramp applied to a sweeping electrode. Temporal shape of the light signal has thus been converted into a spatial distribution of electron flux. The electrons, multiplied in a microchannel plate, then strike a phosphor screen, forming a streak image which may be photographed or viewed with a vidicon.

For intensity and time calibration, a picosecond optical pulse of known pulse energy and duration is allowed to pass through a pair of mirrors before incident on the streak camera. A train of pulses separated in time by $\Delta t=2d/c$, where d is the air separation between the reflecting surfaces and c is the speed of light, emerges as a result of multiple reflections. The intensity decays by $(1-T)^2$, where T is the transmission of a mirror, from one pulse to the subsequent pulse in the train, providing a convenient calibration.

Temporal resolution of a streak camera is determined by a number of factors. For example, photoelectrons emitted from the photocathode at the same time may have different velocities, causing a transit time spread. Finite width of the camera slit causes another spread. Streak cameras with a time resolution better than 2 psec are now commercially available [49].

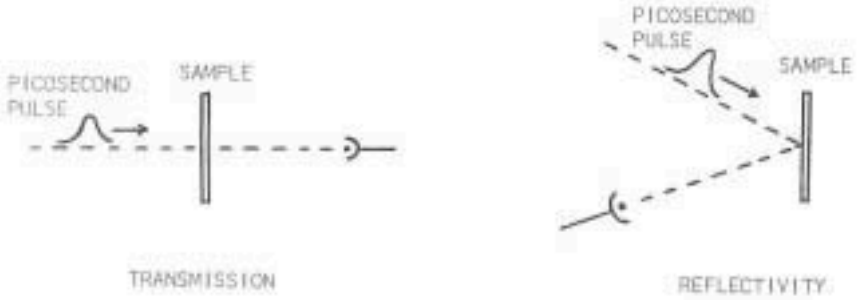

Fig.35. Single pulse experiments.

Experimental arrangements for time-resolved emission studies using streak cameras are simple. For example, Fig.31 shows a setup for recording fluorescence [50]. A picosecond optical pulse is splitted into three. One pulse is used to excite the sample. The fluorescence from the sample is imaged into the slit of the camera. Another pulse, of known temporal separation, is used as a pre-pulse marker. A third pulse, detected by a photodiode, is used to trigger the streak camera. The streak image is viewed with a SIT (silicon-intensified target) camera and displayed on a video monitor. Fig.32 shows a trace of the fluorescence of erythrosin dye in water recorded with this system [50]. The first peak is the pre-pulse marker. Transient absorption in a medium can also be studied with a streak camera. As shown in Fig.33, the transmission of a picosecond laser-excited sample is probed with fluorescence (nanosecond duration) from a laser-excited dye. Yoshihara et al. used this system to study the transient absorption of trans-stilbene [51]. Capability of the streak camera to directly record transient light intensity with pico-

second resolution has made it a desirable tool for ultrafast phenomena studies. The major drawback is its high cost.

3.4 The Population Mixing Method

Population mixing is a recently-developed method for time-resolved light emission studies which does not require a costly streak camera. Unlike the gating by optical mixing technique, critical adjustment of angular alignment is not necessary. Yet it offers a temporal resolution that is optical pulse duration-limited. Fig.34 shows such an experiment by Rosen et al. [52] in the study of time-resolved luminescence from a photo-excited semiconductor. The light source used is a modelocked dye ring laser operated at 610nm and 125 MHz repetition rate, producing 0.5 psec pulses of 40 pJ pulse energy. The pulse train is evenly divided into two beams, one modulated at 1.43 kHz and the other at 2 kHz. Both beams, one of which goes through a variable delay, are focused onto the sample which is p-type GaAs doped at $6\times10^{18}/cm^3$ Zn concentration at 115°K. Photoluminscence at 840nm is collected and imaged into the slit of a spectrometer. An RCA7265 photomultiplier and a PAR lock-in amplifier set at the difference frequency 570 Hz are used for detection. In this manner, only the photoluminescence signal produced by the mixing of the populations created by the beams is measured. Take n(t) and n(t+τ) be the free-carrier populations created by the two beams. Signal detected is

$$I(\tau) \propto \int_{-\infty}^{\infty} n(t)n(t+\tau)dt$$

where τ is the time delay between the excitation pulses. Relaxation behavior of the photogenerated carriers can thus be obtained by varying the delay time. If the carriers decay exponentially with time constant T, then

$$I(t) \propto \exp(-|\tau|/T)$$

This method allows isolation of the fast components of carriers in a heavily doped semiconductor. In the above experiment,

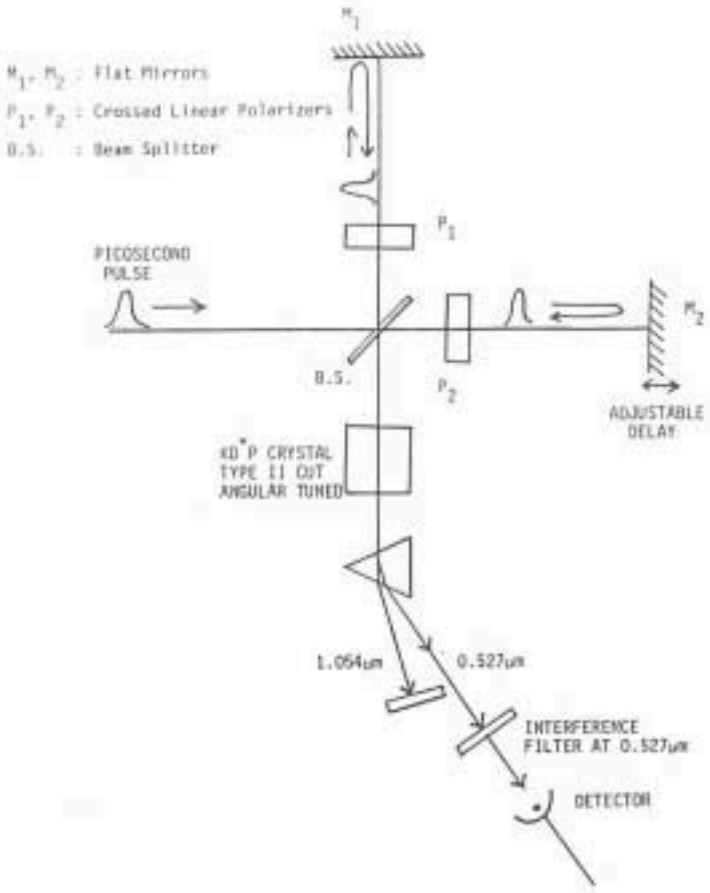

Fig.36. Pulse duration measurement by second harmonic generation.

for example, the density of the photogenerated carriers is estimated to be about $5\times10^{16}/cm^3$, at least two orders of magnitude less than the background density. This technique has proved to be useful in Raman studies [53].

3.5 Single Pulse Measurements

Most of the methods described above require more than one pulse. The simplest experiment is one in which only a single pulse is involved. As illustrated in Fig.35, measurements can be made on the transmission or reflectivity of a sample. This gives information about processes that occur within the duration of the pulse. The first part of the pulse induces a change in the medium which affects the later of the pulse. Nonlinear saturations in semiconductors have been measured by studying the transmissions as a function of the intensity [54,55]. We applied this technique to study the reflectivity of germanium as a function of picosecond irradiance [56,57]. A significant increase in reflectivity at high irradiances was observed, which we interpreted as a contribution to the dielectric function arising from direct-free-hole transitions within the branches of the valence band.

3.6 Optical Pulsewidth Measurements

The streak camera is a useful tool for ultrashort pulse diagnostics. The temporal profile of the intensity of a single pulse can be directly recorded. Special systems offering resolution better than a psec has been built [58,59]. However, the initial high cost prevents it from being a popular tool.

The most common technique used in ultrashort pulse evaluation is autocorrelation measurement by second harmonic generation (SHG). Fig.36 shows a setup we have used. A KD*P crystal cut for type II SHG is used as the nonlinear medium. The pulse measured is splitted into two at the beam splitter. Two crossed linear polarizers P_1 and P_2 are used to make the polarizations of the splitted pulses perpendicular to each other. Second harmonic generation in the crystal occurs only where the two pulses overlap. Thus, by

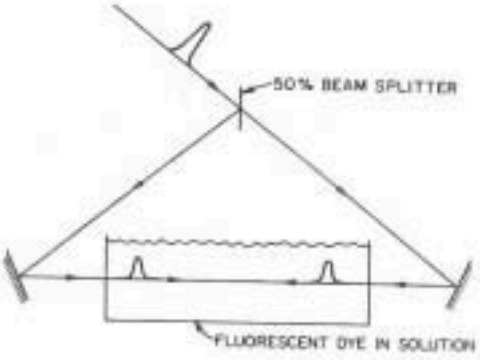

Fig.37. Pulse diagnostic by TPF measurement and a photograph of a fluorescence trace (after [60]).

monitoring the second harmonic green light as one pulse is delayed with respect to the other, the duration of the pulses can be calculated from the signal profile, with an assumed pulse shape.

Another common technique is two-photon-fluorescence (TPF). As shown in Fig.37, an input pulse is splitted into two beams which then traverse an organic dye solution in opposite directions. Fluorescence from the two-photon excited dye is photographed from the side. A densitometer trace of the film reproduces the autocorrelation function of the pulse intensities.

4. Picosecond Opto-Electronic Techniques

The combination of picosecond optical pulses with ultrafast photoconductors has led to new measurement techniques for high speed electronics. In this approach, electronic switches and sampling gates are made with ultrafast photoconductors illuminated by picosecond or subpicosecond optical pulses. Using radiation-damaged silicon-on-sapphire films, opto-electronic switching with a response time less than 8 psec has been demostrated [61]. This powerful technique has been applied in the characterization of high-speed photodetectors and electronic devices.

The first demonstration of picosecond electronic pulse switching using modelocked laser pulses was done by Auston in 1975 [62]. As illustrated in Fig.38, the switch consists of a thin slab of silicon (10^4 Ω-cm) about 0.43mm thick on which an aluminum microstrip transmission line consists of a ground plane and an upper conductor is fabricated. The upper conductor has a gap 0.34mm by 0.34mm. The input coaxial cable on the left is charged to a dc voltage of +20V. With a high resistance in excess of $10^5\Omega$, the gap prevents

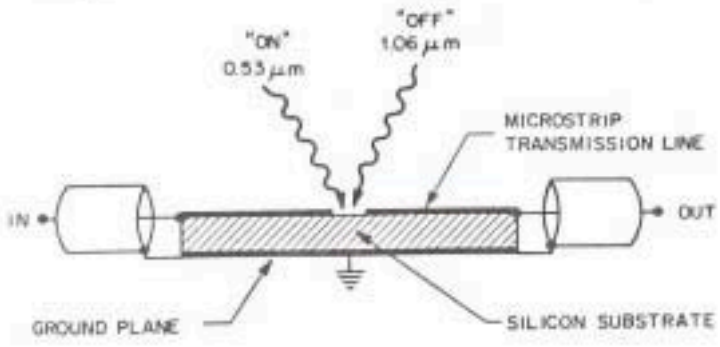

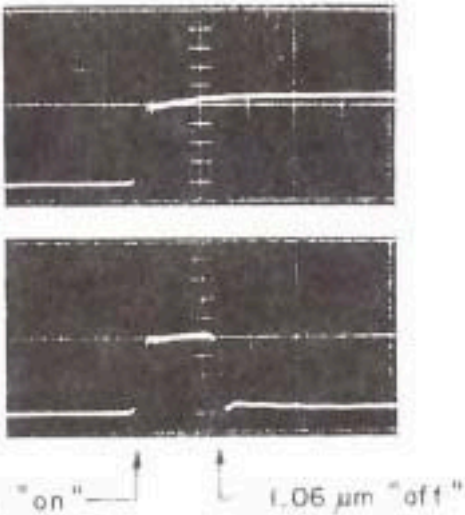

Fig.38. An opto-electronic switch. Horizontal scales in the oscilloscope traces are 3nsec/div. (after [61]).

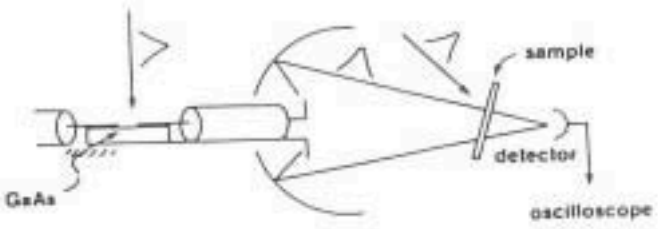

Fig.39. Picosecond microwave pulse generation by subpicosecond laser-activated Cr-doped GaAs switch driving a coaxial cable terminated by a small dipole attenna. The elliptical reflector focuses the microwave burst through a thin Ge-slab to a detector monitored by a fast oscilloscope (after [65]).

transmission of a signal across the device. As shown in the photographs of the oscilloscope traces in Fig.38, initial voltage across the output is negligible.

A 530nm optical pulse of about 5 psec duration incidents on the device at the gap. Since the photon energy (2.34eV) is higher than the direct bandgap of Si, absorption coefficient α ($> 10^4 cm^{-1}$) is high such that all the photons are absorbed by direct interband transitions in a thin layer within 1 micron ($\sim \alpha^{-1}$) of the surface, creating an electron-hole plasma with a carrier density as high as 10^{20} cm^{-3} [28]. A thin layer of high conductivity greater than $10^3(\Omega cm)^{-1}$ is thus produced near the top surface of the crystal. This turns the switch on allowing transmission of a signal as shown in the top photograph of Fig.38.

A 8 psec long optical pulse at 1.06μm containing about the same amount of energy as the turn-on pulse, is used to turn the switch off. In this case, since $h\nu$ is smaller than the bandgap, the pulse is absorbed via indirect absorption and two-photon absorption. The longer absorption depth (hundreds of microns) results in a high conductivity region that extends through the thichness of the crystal to the ground plane. This shorts the transmission line, forbidding further transmission of signal as shown in the lower oscilloscope photograph of Fig.38, which corresponds to a delay of 2.4 nsec of the turn-off pulse with respect to the turn-on pulse. Both optical pulses

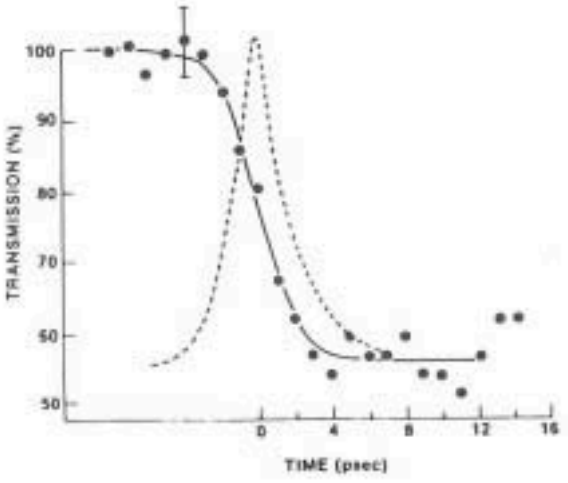

Fig.40. Normalized output from the microwave detector vs time delay between the gating and switching pulses. Time derivative of a smooth curve drawn through the data has a FWHM of 2.8 psec (after [65]).

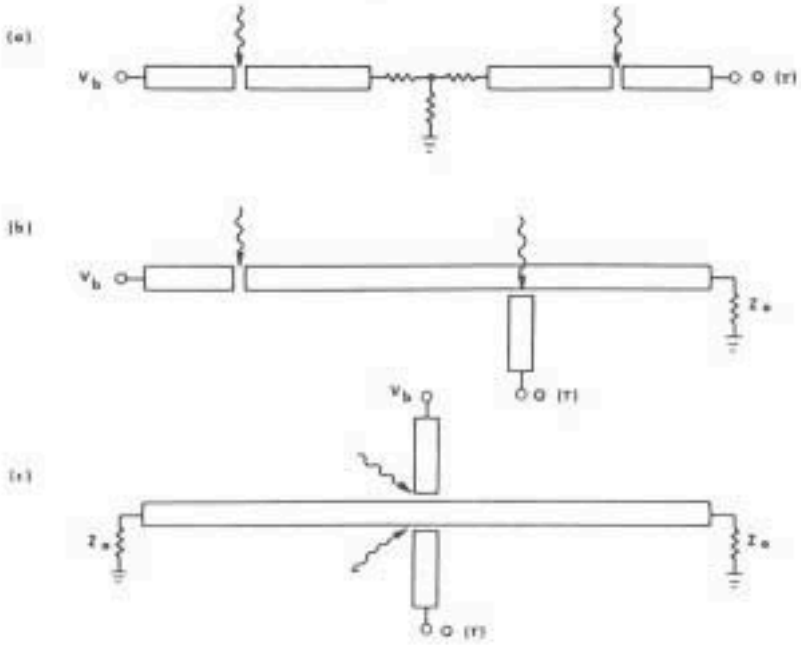

Fig.41. Transmission line electrode patterns used for picosecond opto-electronic correlation measurements. (a) Tandem two-gap correlation scheme; (b) in-line gap and sampling gap; (c) symmetric injecting and sampling gaps on transmission line (after [63]).

are derived from a single pulse switched out from a modelocked train of a Nd: glass laser. The 0.53μm pulse is generated by second harmonic generation in a KDP crystal.

The speed of this device is limited by the combination of a number of factors : optical pulsewidths, bandwidth of the coaxial cables and switch circuit, dielectric relaxation time and RC time constant of the gap. The microstrip structure with a submillimeter substrate thickness has a bandwidth of a few hundred GHz. Since gap capacitance is typically 10^{-14}F, photo-induced conductivities are sufficiently large that both the RC time constant and the dielectric relaxation time constant $\tau=\varepsilon/\sigma$ are less than 1 psec. The intrinsic switching speed is thus primarily limited by the optical pulsewidths.

To determine switching speed of the device, correlation function of the transmission factors of the two gates in tandem was measured. The first gate, biased with a dc voltage,was used to generate a 15 psec long electrical pulse, which propagated down the transmission line. Output from the second gate, which had an aperture time of 15 psec,was displayed on a fast oscilloscope. Signal amplitudes for various delay between the two gates were measured. Accounting for pulse broadening due to dispersion, the response times of the gates were determined to be about 10 psec.

The initial work of Auston [62] has stirred up wide interest in the area of picosecond opto-electronics. Recent progress has led to opto-electronic gates that are switchable at much lower optical intensities and have higher speed. They have been applied towards the switching of microwave and millimeter wave signals, the switching of multi-kilovolt pulses, and the measurement of the response of high speed electro-optical and opto-electronic devices.

As discussed above, a suitable design of switch geometry and circuit results in a device whose speed is optical pulsewidth-limited. In order to

obtain faster speeds, it is thus desirable to use optical pulses of shorter durations. Modelocked dye lasers synchronously pumped by modelocked argon-ion lasers producing optical pulses 2-4 psec in duration [63,64] and subpicosecond pulses generated by cw passively modelocked dye laser systems [65] are typically used. In order to make switches operational with dye lasers, which produce $\sim 10^{-9}$ J pulse energies, and semiconductor diode lasers [66], producing pulses in the 10^{-12} J regime, a small-gap design is necessary. Typical gap widths range from 50 μm down to 3 μm [66].

If the transmission line is not shorted with the application of a second pulse as described in above, switch-off of the device will depend on decay time of the electron-hole plasma due to sweepout or recombination. In the case of Si, this decay time is in excess of a microsecond. The need of a switch-off pulse presents severe limitations on the use of different materials and lasers. In addition, the maximum allowable repetition rate is limited by free-carrier relaxation time. To make switches operable with a single optical pulse, there has been an active search for photoconductive materials with short lifetimes. Semi-insulating Fe-doped InP [66]and Cr-doped GaAs [67], for example, are found to have short lifetimes 50-100 psec. The shortest carrier lifetime ($\sim$ 4 psec) has been found in amorphous silicon films [68]. The extremely fast decay is due to capture of photo-generated carriers from mobile extended states into deep localized states arising from structural defects [63]. However, the amorphous Si device suffers from having a low mobility on the order of 1 cm^2/Vsec. Recently, this situation has been improved by using radiation-damaged silicon-on-sapphire films, which exhibit a slightly longer carrier lifetime of about 8 psec but a carrier mobility at least an order of magnitude higher than amorphous Si [61]. Besides being useful in ultrafast gating of electrical signals, these materials have also been used in making photoconductive detectors with response times below 10 psec [61,68].

With an extremely broadband up to 100 GHz, picosecond opto-electronic devices decribed above are capable of switching microwave and millimeter wave signals. With microwave 1-10GHz, Johnson and Auston demonstrated gating of signals as short as a single rf cycle [69]. Using a dielectric waveguide, Lee et al. succeeded gating millimeter wave signals with frequencies higher than

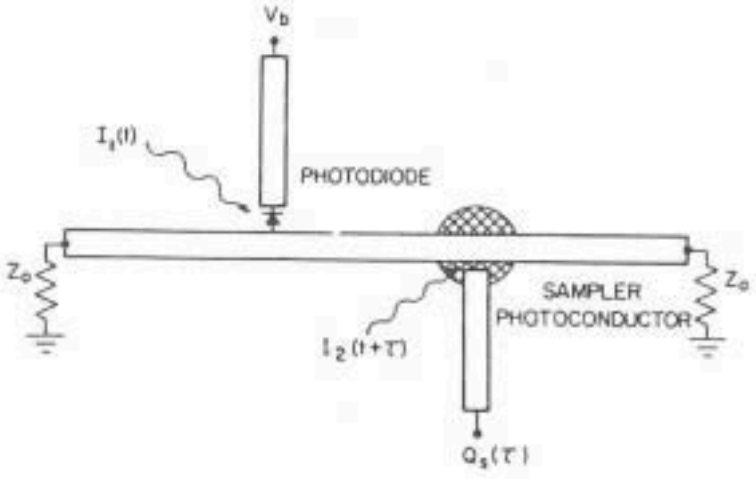

Fig.42. Schemetic diagram of the circuit used in the characterization of a high-speed silicon photodiode. Aperture time of the sampling gate, formed of proton-irradiated GaAs, is approximately 12 psec (after [76]).

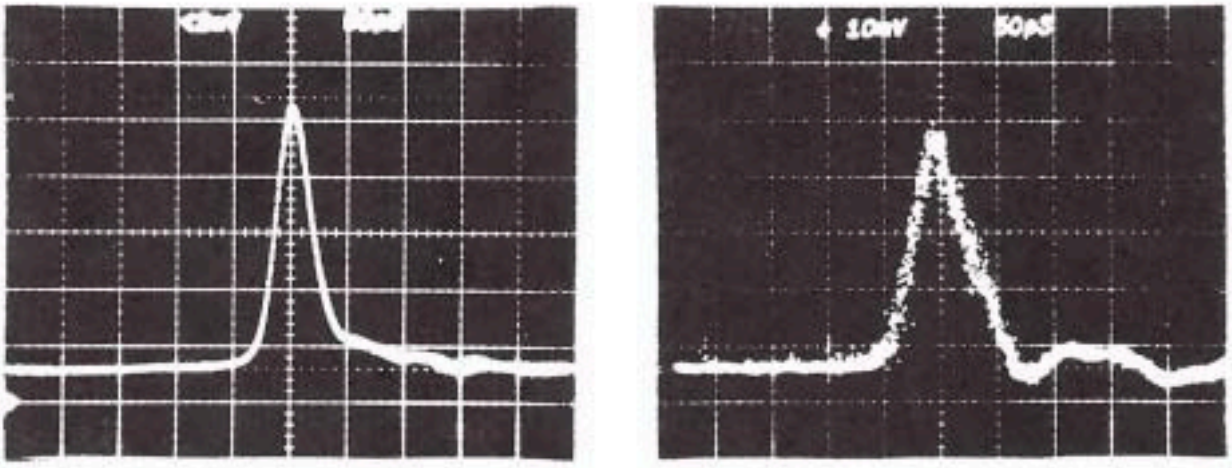

(a) (b)

Fig.43. (a) Photodiode response measured with photoconducting sampling gate. (b) Same photodiode measured on a sampling oscilloscope with a specified rise time of 25 psec. The horizontal scale in these photographs is 50 psec /div (after [63]).

30 GHz [70]. Recently, Mourou et al. [65] demonstrated a method to generate microwave pulses shorter than 3 psec in duration. Their experimental scheme is shown in Fig.39. Short optical pulses, 500 fsec width at 610nm, generated by a cw passively mode-locked dye laser, are amplified to the mJ level by a 10 Hz, actively Q-switched Nd:YAG laser pumped three-stage dye amplifier. Each pulse is splitted into two by a dielectric beam splitter. One of them is used to activate a Cr-doped GaAs photoconductor switch which drives a coaxial cable terminated by a small dipole antenna. Upon illumination, the dc-biased GaAs switch generates a step voltage which propagates down the coaxial cable to pulse the antenna. An elliptical reflector is used to focus the microwave burst, through a Ge slab, at a detector. Upon illumination by the other half of the optical pulse, which generates a dense electron-hole plasma, the thin Ge slab acts as a gate to the microwave. Gate reflectance can be regarded as a step function with a rise time dictated by the optical pulsewidth. The normalized microwave detector output is shown in Fig.40 as a function of time delay between the switching and gating pulses. This is the correlation function between the microwave signal and the gate reflectance, corresponding to the time integral of the microwave burst. Time derivative of the data curve has a FWHM of approximately 2.8 psec, which corresponds to the microwave pulse duration. The generated microwave has an expected central frequency of 800 GHz. Picosecond microwave pulses have potential applications such as precision radar, probing of low density laser-generated plasmas in semiconductors, investigation of photoinduced phase changes in silver halide materials, and generation of quasi-particles in the study of nonequilibrium superconductivity.

Fast switching in silicon has been demostrated up to 1.5 kV by LeFur and Auston [71] and to 10 kV by Antonetti et al. [72]. Si, with a resistivity of $2 \times 10^4 \Omega$cm at room temperature, is not an effective insulator. To avoid thermal dissipation problem, a nanosecond pulse bias is used. Recent experiment

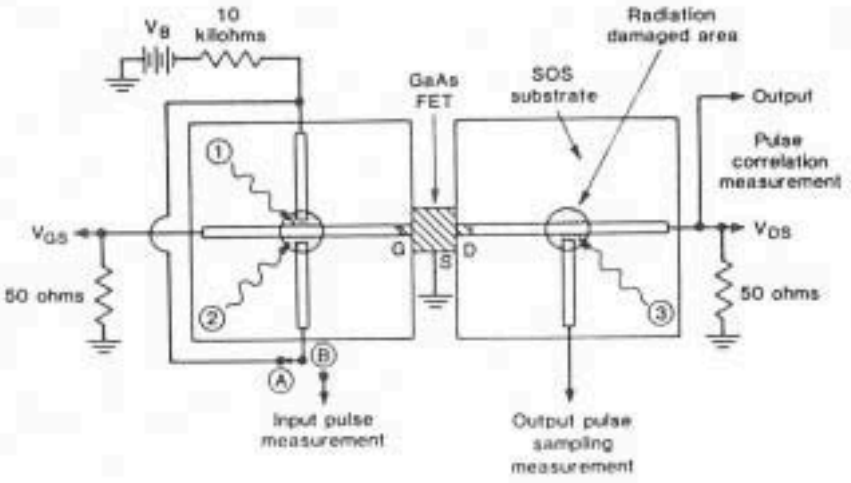

Fig.44. Picosecond opto-electronic measurement of impulse response of a GaAs FET (after [77]).

demonstrated that semi-insulating Cr-doped GaAs (resistivity > $10^7\Omega$cm), with a much less severe thermal instability, can hold off up to 8kV dc and switch with an 90% efficiency [73]. Efficient multi-kilovolt opto-electronic switching in dc-biased $CdS_{0.5}Se_{0.5}$ has also been reported [74]. The high voltage pulse generated has been used to drive a fast Pockels cell [71,73]. The electronic switch-Pockels combination makes an efficient high speed optical switch triggered by light.

4.1 Picosecond Opto-Electronic Sampling and Correlation Measurements

The picosecond photoconductive switch described above has found potential applications in characterization of high speed detectors and electronic devices. Advances in recent years have produced new photoconductors and solid-state devices of tremendous speed. A photoconductor made of amorphous silicon film deposited on fused silica, for example, has a response time less than 40 psec [68]. GaAs and silicon FET's with effective channels less than a micron, as a further example, have propagation delays which are estimated to be 30 psec [75]. Although sampling oscilloscopes with rise times as short as 25 psec exist, trigger jitter, noises and reflections limit their useful speed to approximately 50 psec.

Typical arrangements used are shown in Fig.41, which shows the top views of the transmission line electrode patterns [63]. Two picosecond laser-activated photoconductors are used. The first photoconductor, biased with a dc voltage, acts as a pulse generator. Its output is sampled by the second photoconductor, which is triggered by a delayed optical pulse. If v_1, v_2 are the signals produced by the photoconductors with dc bias, total charge Q measured at the output of the second photoconductor is proportional to the correlation function

$$Q(\tau) \propto \int_{-\infty}^{\infty} v_1(t) v_2(t+\tau) dt$$

where τ is the delay time.

This approach resembles the correlation technique used to measure the response time of the Si photoconductive switch [62]. However, unlike the Si switch which needs two optical pulses for operation, each photoconductor here is switched by a single pulse. The response time is thus determined by the relaxation of the photo-generated free carriers. Besides, each photoconductor here operates in a linear, rather than a saturated regime.

The geometry shown in Fig.41a, called a tandem two-gap autocorrelator circuit, has an impedance-matched attenuator in between, which dampens reflections and ensures that minimal dc bias is applied to the second photoconductor. This geometry has the advantage of being more flexible that samples can be interchanged and cross correlation are possible between unlike samples. In the geometry in Fig.41b, the second photoconductor samples the

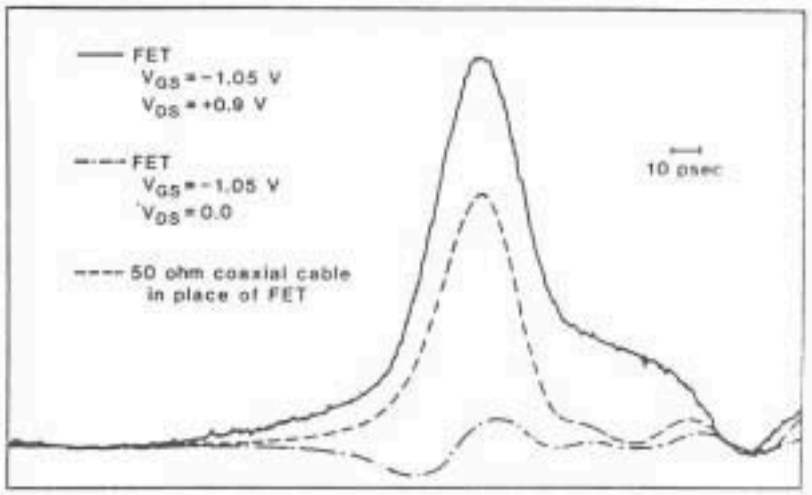

Fig.45. Response of GaAs FET measured using circuit of Fig.44 (after [77]).

electrical signal on the main transmission line produced by the first gap which is dc biased. Since the main line is terminated, an attenuator is not needed to isolate the two conductors. In the scheme of Fig.41c, the biased electrode injects a charge into the main transmission line when the first gap is activated. Served as a load, the main transmission line permits the charge to propagate away rapidly. The second gap, activated by a delayed optical pulse, samples the current before its dissipation. Using high-defect-density amorphous semiconductors such as α-Si, these measurement schemes have shown to be capable of measuring electronic transients with a temporal resolution less than 10 psec [63].

Fig.42 depicts schemetically an opto-electronic sampling circuit used in the characterization of high-speed photodetectors [76]. The photodetector, in this case a silicon p-i-n diode, is mounted on a 50Ω microstrip aluminum transmission line and dc biased at -48V dc. When activated by a picosecond optical pulse, the photo-current is injected into the main transmission line that is terminated at both ends. Gap between the sampling line and the main transmission line has a width of 12 μm. The sampling photoconductor is a small chip of semi-insulating GaAs which has been irradiated with $3x10^{15}$

protons /cm^2 at 300 keV. Carrier relaxation time, as estimated from cross-sections of electron traps, is about 3 psec. Optical pulses of $\sim$ 4 psec duration from a synchronously pumped, modelocked R6G dye laser operating at 580 nm and 82MHz repetition rate are used to operate the device. Since the two pulses used to activate the photodiode and the sampling gate are splitted from the same beam, and time delay is produced to high precision with a varible optical path, time jittering in synchronization between photoconductor and and sampling gate is essentially eliminated.

Response of the photodiode measured with the photoconducting sampling gate is depicted in Fig.43a, showing a FWHM of 36 psec. For comparison, the response of the same diode, under the same optical power and bias voltage, is measured with a sampling oscilloscope with a specified rise time of 25 psec (Fig.43b). The sampling oscilloscope result shows a FWHM of 55 psec, indicating considerable instrument broadening. The photograph clearly indicates that noise level and reflection are also much severe in the sampling oscilloscope. Using an autocorrelation measurement, aperture of the photoconducting sampler has been estimated to be about 12 psec.

The photoconducting sampling gate has found applications in direct probing of high-speed solid-state electronic devices. Fig.44 illustrates the first experiment of this kind, performed by Smith et al. in 1981, in which the impulse response of a GaAs microwave field effect transistor (FET) is studied with a time resolution better than 10 psec [79]. One micron thick silicon-on-sapphire films, bombarded with argon ions at 2 MeV, are used as photoconductors. Short electrical pulses, generated by applying a dc bias V_B to the side microstrip line and illuminating photoconductor 1, as shown in Fig.44, are applied to the gate of the FET. These pulses are measured by illuminating photoconductor 2 so that it acts as a sampling gate. Impulse response of the FET is then measured with photoconductor 1 generating electrical pulses and photoconductor 3 being activated to sample the output of the FET. To obtain a circuit response for comparison, the same measurement is repeated with a 50Ω coaxial cable in place of the FET. Typical results of these measurements are shown in Fig.45. The dashed line, measured with the FET replaced by a coaxial cable, represents the system response which has a FWHM of 33 psec. The dashed-dot curve shows the capacitively coupled response when the FET is measured without a drain-source bias. With a dc drain-source bias, a net gain is obtained (solid curve). The signal reveals two components : one with a FWHM of 40 psec is almost as fast as the circuit response, and a slower tail indicating a fall time of about 75 psec.

These examples demonstrate that photoconductive sampling is a powerful technique for the evalution of high-speed solid-state devices. Time resolution ($\sim$ 10 psec) is better than the fastest existing sampling oscilloscope. It is essentially jitter-free, and has excellent signal-to-noise properties. In addition, this method can be used in remote environments such as low temperature cryostats without requiring high speed interface [78]. The technique can be readily applied to measurements of a wide variety of devices and materials. Instead of dye lasers, a modelocked semiconductor laser can be used to make a compact integrated device. With further improvement in the speed of photoconducting materials and circuits, using shorter optical pulses, it is expected the time resolution of these opto-electronic measurement systems can reach 1 psec [79].

Achnowledgements

The author acknowledges partial support by National Science Council, Republic of China.

References

1. S.L. Shapiro, in Ultrashort Light Pulses, ed. S. L. Shapiro (Springer-Verlag, Berlin-Heidelberg-New York, 1977)p.1
2. E. P. Ippen and C. V. Shank, Appl. Phys. Lett. 27, 488 (1975)
3. R. L. Fork, B. I. Green, and C. V. Shank, Appl. Phys. Lett. 38, 671 (1981)
4. G. A. Mourou and S. Sizer II, Opt. Commun. 41, 47 (1982)
5. E. P. Ippen, in Opto-Electronics, ed. K. Young (The Chinese University Press, Hong Kong, 1983)p.155
6. H. W. Mocker and R. J. Collins, Appl. Phys. Lett. 7, 270 (1965)
7. A. J. DeMaria, D. A. Stetser, and H. Heynau, Appl. Phys. Lett. 8, 174 (1966)
8. E. G. Arthurs, D. J. Bradley, and A. G. Roddie, Appl. Phys. Lett. 19, 480 (1971)
9. E. G. Arthurs, D. J. Bradley, and A. G. Roddie, Appl. Phys. Lett. 20, 125 (1972)
10. R. S. Adrin, E. G. Arthurs, D. J. Bradley, A. G. Roddie, and J. R. Taylor, Opt. Commun. 12, 136 (1974)
11. E. P. Ippen, C. V. Shank, and A Dienes, Appl. Phys. Lett. 21, 348 (1972)
12. C. V. Shank, R. L. Fork, R. Yen, R. H. Stolen, and W. J. Tomlinson, Appl. Phys. Lett. 40, 761 (1982)
13. A Yariv, Introduction to Optical Electronics, 2nd edition (Holt, Rinehart and Winston, 1976)
14. C. Y. Leung and T. W. Nee, in Picosecond Phenomena III, eds. K. B. Eisenthal, R. M. Hochstrasser, W. Kaiser, and A Laubereau (Springer-Verlag, Berlin-Heidelberg-New York, 1982)p.380
15. C. V. Shank and E. P. Ippen, Appl. Phys. Lett. 26, 62 (1975)
16. J. Herman, F. Weidner, and B. Wilkelmi, Appl. Phys. B26, 147 (1981)
17. C. V. Shank, R. L. Fork, and R. T. Yen, in Picosecond Phenomena III, eds. K. B. Eisenthal, R. M. Hochstrasser, W. Kaiser, and A. Laubereau (Springer-Verlag, Berlin-Heidelberg-New York, 1982)p.2
18. J. M. Halbout and C. L. Tang, Appl. Phys. Lett. 40, 765 (1982)
19. E. B. Treacy, IEEE J. QE-5, 454 (1969)
20. E. B. Treacy, Phys. Lett. 28A, 34 (1968)
21. E. B. Treacy, Appl. Phys. Lett. 14, 112 (1969)
22. R. L. Fork, C. V. Shank, and R. T. Yer, Appl. Phys. Lett. 41, 273 (1982)
23. G. B. Busch, R. P. Jones, and P. M. Rentzepis, Chem. Phys. Lett. 18, 178 (1973)
24. H. Tashiro and T. Yajima, Chem. Phys. Lett. 25, 582 (1974)
25. D. Magde, B. A. Bushaw, and M. W. Windsor, Chem. Phys. Lett. 28, 263 (1974)
26. R. L. Fork, C. V. Shank, R. T. Yen, and C. Hirlmann, in Picosecond Phenomena II, eds. K. B. Eisenthal, R. M. Hochstrasser, W. Kaiser, and A. Laubereau (Springer-Verlag, Berlin-Heidelberg-New York, 1982)p.10

27. J. W. Shelton and J. A. Armstrong, IEEE J. QE-3, 302 (1967)
28. D. H. Auston and C. V. Shank, Phys. Rev. Lett. 32, 1120 (1974)
29. J. A. Valdmanis, G. Mourou, and C. W. Gabel, in Picosecond Phenomena III, eds. K. B. Eisenthal, R. M. Hochstrasser, W. Kaiser, and A. Laubereau (Springer-Verlag, Berlin-Heidelberg-New York, 1982)p.101
30. C. V. Shank and D. H. Auston, Phys. Rev. Lett. 34, 479 (1975)
31. E. P. Ippen and C. V. Shank, in Ultrashort Light Pulses, ed. S. L. Shapiro (Springer-Verlag, Berlin-Heidel-New York, 1977)p.83
32. A. Laubereau, A Fendt, A Seilmeir, and W. Kaiser, in Picosecond Phenomena, eds. C. V. Shank, E. P. Ippen, and S. L. Shapiro (Springer-Verlag, Berlin-Heidelberg-New York, 1978)p.89
33. G. A. Massey and R. A. Elliott, IEEE J. QE-10, 899 (1974)
34. M. Malley, in Creation and Detection of the Excited State, ed. W. R. Ware (Marcel Dekker, 1974)Vol.2
35. R. L. Fork, C. V. Shank, A. M. Glass, A. Migus, M. A. Bosch, and J. Shah, Phys. Rev. Lett. 43, 394 (1979)
36. R. L. Fork, C. V. Shank, A. M. Glass, A Migus, M. A. Bosch, and J. Shah, J. Non-Crystalline Solids, 35, 963 (1980)
37. D. W. Phillion, D. J. Kuizenga, and A. E. Siegman, Appl. Phys. Lett. 27, 85 (1975)
38. S. C. Moss, J. R. Lindle, H. J. Mackey, and A. L. Smirl, Appl. Phys. Lett. 39, 227 (1981)
39. M. A. Duguay and J. W. Hansen, Appl. Phys. Lett. 15, 192 (1969)
40. M. A. Duguay, Am. Scient. 59, 550 (1971)
41. M. A. Duguay and A. T. Mattick, Appl. Opt. 10, 2162 (1971)
42. R. R. Alfano, S. L. Shapiro, and M. Pope, Opt. Commun. 9, 388 (1973)
43. W. Yu, P. P. Ho, R. R. Alfano, and M. Seibert, Biochimica et Biophysica Acta 387, 159 (1975)
44. E. P. Ippen and C. V. Shank, Appl. Phys. Lett. 26, 92 (1975)
45. H. Mahr and M. D. Hirsch, Opt. Commun. 13, 96 (1975)
47. E. P. Ippen and C. V. Shank, in Picosecond Phenomena, eds. C. V. Shank, E. P. Ippen, and S. L. Shapiro (Springer-Verlag, Berlin-Heidelberg-New York, 1978)p.103
46. K. Mochizuki, Y. Namihira, and Wakabayashi, IEEE J. QE-18, 278 (1982)
48. J. M. Wiesenfeld and E. P. Ippen, Chem. Phys. Lett. 67, 213 (1979)
49. N. H. Schiller, Y. Tsuchiya, E. Inuzuka, Y. Suzuki, K. Kinoshita, K. Kamiya, H. Iida, and R. R. Alfano, Optical Spectra 14-6, 55 (June 1980)
50. W. Yu, F. Pellegrino, M. Grant, and R. R. Alfano, J. Chem. Phys. 67, 1766 (1977)
51. K. Yoshihara, A. Namika, M. S. Sumitani, and N. Nakashira, J. Chem. Phys. 71, 2892 (1979)
52. D. Rosen, A. G. Doukas, Y. Budansky, A. Katz, and R. R. Alfano, Appl. Phys. Lett. 39, 935 (1981)
53. D. von der Linde, J. Kulh, and H. Klingenberg, Phys. Rev. Lett. 44, 1505 (1980)
54. C. J. Kennedy, J. C. Matter, A. L. Smirl, H. Weichel, F. A. Hopf, and S. V. Pappu, Phys. Rev. Lett. 32, 419 (1974)
55. A. L. Smirl, J. C. Matter, A. Elci, and M. O. Scully, Opt. Commun. 16, 118 (1976)
56. B. Bosacchi, C. Y. Leung, and M. O. Scully, Opt. Commun. 27, 475 (1978)
57. B. Bosacchi, C. Y. Leung, M. O. Scully, in Picosecond Phenomena, eds. C. V.Shank, E. P. Ippen, and S. L. Shapiro (Springer-Verlag, Berlin-Heidelberg-New York, 1978)p.244

58. D. J. Bradley and W. Sibbett, Appl. Phys. Lett. 27, 382 (1975)
59. D. J. Bradley, in Proc. 11th Intern. Cong. High Speed Photo., ed. P. J. Rolls (Chapman and Hall, London 1974)p.23
60. P. W. Smith, M. A. Duguay, and E. P. Ippen, in Progress in Quantum Electronics, Vol.3, Pt.2 (Pergaman Press 1974)
61. P. R. Smith, D. H. Auston, A. M. Johnson, and W. M. Augustyniak, Appl. Phys. Lett. 38, 47 (1981)
62. D. H. Auston, Appl. Phys. Lett. 26, 101 (1975)
63. D. H. Auston, A. M. Johnson, P. R. Smith, and J. C. Bean, Appl. Phys. Lett. 37. 371 (1980)
64. A. P. DeFonzo, Appl. Phys. Lett. 39, 480 (1981)
65. G. Mourou, C. V. Stancampiano, A. Antonetti, and A. Orszag, Appl. Phys. Lett. 39, 295 (1981)
66. F. J. Leonberger and P. F. Moulton, Appl. Phys. Lett. 35, 712 (1979)
67. V. K. Mathur and S. Rogers, Appl. Phys. Lett. 31, 765 (1977)
68. D. H. Auston, P. Lavallard, N. Sol and D. Kaplan, Appl. Phys. Lett. 36, 66 (1980)
69. A. M. Johnson and D. H. Auston, IEEE J. QE-11, 283 (1975)
70. C. H. Lee, P. S. Mak, and A. P. DeFonzo, IEEE J. QE-16, 277 (1980)
71. P. LeFur and D. Auston, Appl. Phys. Lett. 28, 21 (1976)
72. A. Antonetti, M. M. Malley, G. Mourou, and A. Orszag, Opt. Commun. 23, 435 (1977)
73. G. Mourou and W. Knox, Appl. Phys. Lett. 35, 492 (1979)
74. V. K. Mathur, C. S. Chang, W. L. Cao, M. J. Rhee, and C. H. Lee, IEEE J. QE-18, 205 (1982)
75. P. Mizutani, N. Kato, S. Ishida, K. Osafune, and M. Ohmori, Electron. Lett. 16, 315 (1980)
76. D. H. Auston and P. R. Smith, Appl. Phys. Lett. 41, 599 (1982)
77. P. R. Smith, D. H. Auston, and W, M. Augustyniak, Appl. Phys. Lett. 39, 739 (1981)
78. D. H. Auston and P. R. Smith, Appl. Phys. Lett. B28, 249 (1982)
79. C. V. Shank and D. H. Auston, Science 215, 797 (1982)